Cell Biology

The RAB27A effector SYTL5 regulates mitophagy and mitochondrial metabolism

Reviewed Preprint
v2 • October 10, 2025
Revised by authors

Reviewed Preprint
v1 • February 17, 2025

Ana Lapao, Lauren Sophie Johnson, Laura Trachsel-Moncho, Samuel J Rodgers, Sakshi Singh, Matthew Yoke Wui Ng, Sigve Nakken, Eeva-Liisa Eskelinen, Anne Simonsen

Department of Molecular Medicine, Institute of Basic Medical Sciences, Faculty of Medicine, University of Oslo, Oslo, Norway • Centre for Cancer Cell Reprogramming, Institute of Clinical Medicine, Faculty of Medicine, University of Oslo, Oslo, Norway • Department of Molecular Cell Biology, Institute for Cancer Research, Oslo University Hospital Montebello, Oslo, Norway • Department of Tumour Biology, Institute for Cancer Research, Oslo University Hospital, Oslo, Norway • Department of Informatics, University of Oslo, Oslo, Norway • Institute of Biomedicine, University of Turku, Turku, Finland

eLife Assessment

This study by Lapao et al. uncovers a novel role for the Rab27A effector SYTL5 in regulating mitochondrial function and mitophagy under hypoxic conditions. Using a range of imaging and functional assays, the authors demonstrate that SYTL5 localizes to mitochondria in a Rab27A-dependent manner and impacts mitochondrial respiration and metabolic reprogramming. While the findings are **solid** and **valuable** in the area of cancer biology, further mechanistic clarity and improved imaging would strengthen the conclusions.

https://doi.org/10.7554/eLife.105541.2.sa4

Abstract

SYTL5 is a member of the Synaptotagmin-Like (SYTL) protein family that differs from the Synaptotagmin family by having a unique N-terminal Synaptotagmin homology domain that directly interacts with the small GTPase RAB27A. Several SYTL protein family members have been implicated in plasma membrane transport and exocytosis, but the specific function of SYTL5 remains unknown. We here show that SYTL5 is a RAB27A effector and that both proteins localise to mitochondria and vesicles containing mitochondrial material. Mitochondrial recruitment of SYTL5 depends on its interaction with functional RAB27A. We demonstrate that SYTL5-RAB27A positive vesicles containing mitochondrial material, autophagy proteins and LAMP1 form during hypoxia and that depletion of SYTL5 and RAB27A reduces mitophagy under hypoxia mimicking conditions, indicating a role for these proteins in mitophagy. Indeed, we find that SYTL5 interacts with proteins involved in vesicle-mediated transport and cellular response to stress and that its depletion compromises mitochondrial respiration and increases glucose uptake. Intriguingly, SYTL5 expression is significantly reduced in tumours of the adrenal gland, and correlates positively with survival for patients with adrenocortical carcinoma.

Introduction

The Synaptotagmin-Like (SYTL) protein family consists of 5 members (SYTL1-5), each containing an N-terminal Synaptotagmin homology domain (SHD) and two C-terminal C2 lipid-binding domains. The SHD domains of SYTL1-5 have been found to directly interact with the small GTPase protein RAB27[1,2]. The C2 domain is generally involved in phospholipid binding and interacts with cellular membranes[3], either in a calcium-dependent or calcium-independent manner[3,4]. Calcium was shown to be required for SYTL3 and SYTL5 phospholipid binding activity[1,5], whereas SYTL2 binding to phosphatidylserine (PS) was inhibited by calcium[6].

The SYTL protein family is generally involved in plasma membrane transport and exocytosis[2,4], mostly through their binding to RAB27 proteins. The main functions of RAB27 are related to vesicle budding, delivery, tethering and fusion with membranes[7] and its activity is regulated by a cyclic activation and inactivation state depending on it binding to guanosine-5'-triphosphate (GTP) or guanosine diphosphate (GDP), respectively[7]. RAB27A and RAB27B are the two RAB27 isoforms found in vertebrates[7] and their binding to effector proteins occurs only when they are bound to GTP[7]. SYTL5 binds to the GTP-bound RAB27A form, indicating its possible role in membrane trafficking events[1].

Functional mitochondria are fundamental for normal cellular metabolism. Mitochondria are the primary source of adenosine triphosphate (ATP) obtained through oxidative phosphorylation (OXPHOS), and are important for cellular calcium homeostasis, lipid metabolism, reactive oxygen species (ROS) generation, and detoxification[8]. Mitochondria can integrate and generate signalling cues to adjust their metabolism and biogenesis to maintain cellular homeostasis[8,9]. Mitochondrial function and health are tightly regulated by several quality control processes involving targeting of parts of mitochondria to lysosomes for degradation, including macromitophagy[10,11] (selective degradation of mitochondria by autophagy), piecemeal mitophagy[12,13], mitochondrial-derived vesicles (MDVs)[14,15], and vesicles derived from the inner mitochondrial membrane (VDIMs)[16]. It has also been found that damaged mitochondria can be directly released to the extracellular space[17], either contained within extracellular vesicles[18] or by mitocytosis, where damaged mitochondria are expelled in migrasomes[19].

Exposure of mitochondria to various stressors can affect their function and lead to severe diseases, such as neurodegenerative disorders and cancer[20,21]. Cancer cells can trigger a change in mitochondrial metabolism to promote cell proliferation and survival by a process known as the Warburg effect, characterised by a switch from OXPHOS to ATP production through glycolysis even under normoxic conditions[22]. Adrenocortical carcinoma (ACC) is a rare type of cancer that develops in the adrenal gland cortex, having a very poor prognosis and limited treatment options[23]. Most patients are diagnosed at advanced cancer stages and present an excess in adrenocortical hormone production[23]. Mitochondria are known to be essential organelles in the synthesis of steroid hormones, including cortisol, since they contain specific enzymes that catalyse steroid synthesis from cholesterol delivered to the mitochondria[24].

Here we demonstrate that SYTL5 localises to mitochondria in a RAB27A-dependent manner and that both proteins regulate mitophagy and cellular metabolism. Cells lacking SYTL5 undergo a shift from mitochondrial oxygen consumption to glycolysis, which may explain the correlation between low SYTL5 expression and poor survival of ACC patients.

Results

SYTL5 localises to mitochondria and endolysosomal compartments

SYTL5 was identified as a putative candidate in a screen for lipid-binding proteins involved in the regulation of mitophagy[25]. To characterise the cellular localisation and function of SYTL5, we generated U2OS cells with stable inducible expression of SYTL5-EGFP as there are no antibodies recognising endogenous SYTL5 and our efforts to tag endogenous SYTL5 using CRISPR/Cas9 were also unsuccessful. Intriguingly, live cell imaging analysis revealed that SYTL5-EGFP co-localised with filamentous structures positive for MitoTracker red (**Figure 1A**), which labels active mitochondria. Moreover, several SYTL5-EGFP positive vesicles were observed, including some small and highly mobile SYTL5-EGFP vesicles moving along the mitochondrial network (**Supplementary video 1 and arrows in Figure 1B**). SYTL5-EGFP staining at the plasma membrane was also seen, particularly in cells with higher expression levels (**Figure 1C**), which may suggest a role for SYTL5 in secretion to the plasma membrane.

To determine the identity of the SYTL5 positive vesicles, U2OS SYTL5-EGFP cells were infected with a panel of lentiviral RAB GTPase constructs representing different cellular compartments (**Supplementary Figure 1A-F**) and analysed by live cell imaging. SYTL5-EGFP positive structures were observed to co-localise with vesicles positive for RAB4 and RAB11, two GTPases that mainly localise to recycling endosomes[26] and to some extent with RAB5, mostly localised to early endosomes[26] (**Supplementary Figure 1A-C**). Co-localisation was also observed with RAB7, a marker of late endosomes, lysosomes and autophagosomes[26] and partially with RAB9, which associates with late endosomes and mediates the transport between late endosomes and the *trans*-Golgi network[26] (**Supplementary Figure 1D-E**). SYTL5-EGFP showed little or no co-localisation with RAB6 positive structures, representing Golgi-derived vesicles (**Supplementary Figure 1F**). In line with an endocytic identity of SYTL5-EGFP positive vesicles, they were also positive for lysosomal markers, including LysoTracker red, which labels acidic compartments in the cell (**Figure 1C**), and the lysosomal membrane marker LAMP1 (**Figure 1D**).

Thus, based on live cell imaging analysis we conclude that SYTL5 localises to the mitochondrial network and to mitochondria-associated vesicles that partly overlap with endolysosomal compartments.

Mitochondrial localisation of SYTL5 requires both the RAB27-binding SHD domain and the lipid-binding C2 domains

To investigate whether the observed intracellular localisation of SYTL5-EGFP depends on its binding to RAB27 and/or lipids, we generated U2OS cells with stable expression of EGFP-3xFLAG-tagged wild type SYTL5 or SYTL5 lacking either the RAB27-binding SHD domain (SYTL5(ΔSHD)) or the two lipid-binding C2 domains (SYTL5(ΔC2AB)) (**Figure 1E**).

To validate the SYTL5(ΔC2AB) mutant and determine the lipid-binding specificity of SYTL5, lysates from these cells were incubated with membranes containing various phosphoinositides and other lipids. Full-length SYTL5 was observed to bind to mono-phosphorylated phosphoinositides (PI(3)P, PI(4)P, PI(5)P), as well as PI(4,5)P2, PI(3,4,5)P3 and to some extent to phosphatidic acid (PA) and cardiolipin (CL) (**Figure 1F**). As expected, upon removal of the C2 domains, specific binding to all lipid species was lost, while SYTL5 lacking the SHD domain retained the ability to bind to lipids (**Figure 1F**).

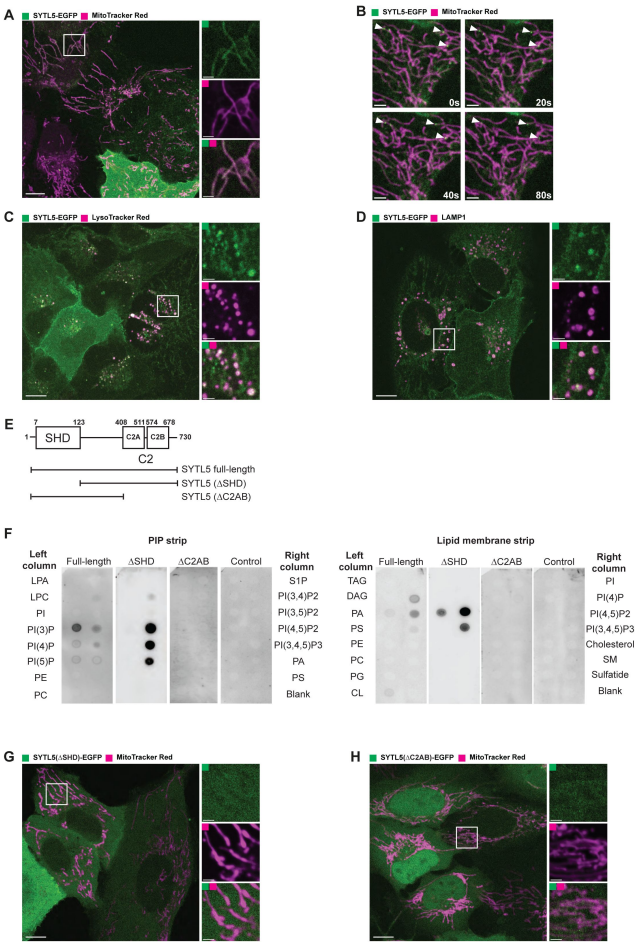

Figure 1.

Lipid binding protein SYTL5 localises to mitochondria and endo-lysosomes

A. Live confocal microscopy imaging of U2OS stably expressing SYTL5-EGFP co-stained with 50 nM MitoTracker red. SYTL5-EGFP expression was induced for 24 h using 100 ng/ml doxycycline. MitoTracker red was added 30 min before imaging. Scale bars: 10 µm, 2 µm (insets).
B. Time-lapse video frames (Supplementary video 1) tracking SYTL5 vesicle movement along filaments positive for MitoTracker red (arrows). SYTL5-EGFP expression was induced for 24 h using 100 ng/ml doxycycline. Scale bars: 3 µm.
C. Live confocal microscopy imaging of U2OS stably expressing SYTL5-EGFP co-stained with 50 nM LysoTracker red. SYTL5-EGFP expression was induced for 24 h using 100 ng/ml doxycycline. LysoTracker red was added 30 min before imaging. Scale bars: 10 µm, 2 µm (insets).
D. Confocal imaging of U2OS stably expressing SYTL5-EGFP stained for endogenous LAMP1. Nuclei were stained using Hoechst. Scale bars: 10 µm, 2 µm (insets).
E. Overview of domain structure of SYTL5 full length, ΔSHD and ΔC2AB mutants.
F. 3xFLAG fusion proteins expressed in U2OS cells (SYTL5-EGFP-3xFLAG, SYTL5 (ΔSHD)-EGFP-3xFLAG and SYTL5 (ΔC2AB)-EGFP-3xFLAG) were immunoprecipitated and added to membranes spotted with lipids found in cell membranes: LPA (lipoprotein A); LPC (lysophosphatidylcholine); PI (phosphatidylinositol); PI(3)P (phosphatidylinositol 3-phosphate); PI(4)P (phosphatidylinositol 4-phosphate); PI(5)P (Phosphatidylinositol 5-phosphate); PE (phosphatidylethanolamine); PC (phosphatidylcholine); S1P (sphingosine-1-phosphate); PI(3,4)P2 (phosphatidylinositol 3,4-bisphosphate); PI(3,5)P2 (phosphatidylinositol 3,5-bisphosphate); PI(4,5)P2 (phosphatidylinositol 4,5-bisphosphate); PI(3,4,5)P3 (phosphatidylinositol 3,4,5 –triphosphate); PA (phosphatidic acid); PS (Phosphatidylserine); TAG (triglyceride); DAG (diglyceride); PG (phosphatidylglycerol); CL (cardiolipin); Cholesterol; SM (sphingomyelin); Sulfatide.
G. Live confocal microscopy imaging of U2OS stably expressing SYTL5 (ΔSHD)-EGFP-3xFLAG co-stained with 50 nM MitoTracker red added 30 min before imaging. Scale bars: 10 µm, 2 µm (insets).
H. Live confocal microscopy imaging of U2OS stably expressing SYTL5 (ΔC2AB)-EGFP-3xFLAG co-stained with 50 nM MitoTracker red added 30 min before imaging. Scale bars: 10 µm, 2 µm (insets).

The SYTL5(ΔSHD)-EGFP and SYTL5(ΔC2AB)-EGFP expressing cell lines were then incubated with MitoTracker red and analysed by live cell imaging. Indeed, the SYTL5 colocalisation to mitochondria was lost and both SYTL5(ΔSHD)-EGFP and SYTL5(ΔC2AB)-EGFP were dispersed in the cytosol (**Figure 1G-H**), indicating that both the RAB27-interacting SHD domain and the lipid binding C2 domains are required for mitochondrial localisation of SYTL5.

Mitochondrial localisation of SYTL5 requires RAB27A GTPase activity

Given that the SHD domain of SYTL5 has been shown to bind RAB27A[1] and our observations that the SHD domain is required for mitochondrial localisation of SYTL5, we asked whether RAB27A activity is required for SYTL5 recruitment to mitochondria. U2OS SYTL5-EGFP cells were infected with a mScarlet-RAB27A lentiviral construct to generate a stable cell line. Co-expression of SYTL5-EGFP and mScarlet-RAB27A resulted in a clear co-localisation of both proteins to filaments positive for MitoTracker DeepRed (DR) (**Figure 2A**). The mitochondrial localisation of SYTL5-EGFP and mScarlet-RAB27A was confirmed by correlative light and EM (CLEM) analysis using the same cell line (**Figure 2B, zoom in 1**). Intriguingly, the mitochondrial localisation of SYTL5-EGFP was enhanced when co-expressed with mScarlet-RAB27A compared to cells expressing SYTL5-EGFP only (**Figure 1A-B**), indicating that RAB27A might facilitate mitochondrial recruitment of SYTL5. Indeed, in U2OS cells with stable expression of mScarlet-RAB27A only, RAB27A strongly co-localised with MitoTracker green (**Supplementary Figure 2A**), demonstrating its mitochondrial targeting. Moreover, SYTL5-EGFP and mScarlet-RAB27A were both detected in the mitochondrial fraction (containing TIM23 and COXIV) of cells expressing SYTL5-EGFP or mScarlet-RAB27A (**Supplementary Figure 2B**). Importantly, the mitochondrial localisation of SYTL5 and RAB27A is not specific to U2OS cells as HeLa cells with stable expression of SYTL5-EGFP or mScarlet-RAB27A show a similar expression pattern to U2OS cells, as demonstrated by co-localisation of SYTL5-EGFP with MitoTracker Red and plasma membrane staining in cells having higher expression (**Supplementary Figure 2C**) and of mScarlet-RAB27A with MitoTracker Green (**Supplementary Figure 2D**). All further experiments were conducted in U2OS cells.

To further characterise mitochondrial recruitment of SYTL5 and RAB27A and elucidate their role at the mitochondrion, we used CRISPR/Cas9 to knock out (KO) RAB27A and SYTL5 in U2OS cells (**Supplementary Figure 3A-D**). This double-KO (dKO) cell line was further transduced with lentiviral constructs to constitutively express SYTL5-EGFP, mScarlet-RAB27A, or both, and their mitochondrial localisation was analysed by live cell imaging (**Figure 2C-E**). Intriguingly, mScarlet-RAB27A co-localised extensively with MitoTracker green and to small vesicles dispersed in the cytoplasm and located at or near mitochondria (**Figure 2C**), indicating that SYTL5 is not required for RAB27A mitochondrial localisation. In contrast, SYTL5-EGFP was not recruited to mitochondria when expressed alone in dKO cells, although some SYTL5-EGFP vesicles were seen near mitochondrial structures (**Figure 2D**). Upon co-expression of SYTL5-EGFP and mScarlet-RAB27A in dKO cells the mitochondrial localisation of SYTL5-EGFP was rescued (**Figure 2E**), demonstrating that mitochondrial recruitment of SYTL5 is dependent on RAB27A.

Since SYTL5 has previously been described as a RAB27A effector[1], we asked whether its mitochondrial recruitment depends on binding to the GTP-bound form of RAB27A. To address this, dKO cells expressing SYTL5-EGFP were rescued with the constitutively active (RAB27A-Q78L) or inactive (RAB27A-T23N) mutant forms of mScarlet-RAB27A. As expected, SYTL5-EGFP interacted specifically with RAB27A wild type (WT) and RAB27A-Q78L, as well as with endogenous RAB27A in control cells, while no interaction was detected with RAB27A-T23N, as assessed by GFP-pulldown (**Figure 2F**). To our surprise, live cell imaging of the same cells revealed that, in contrast to mScarlet-RAB27A WT, neither the RAB27A Q78L nor the T23N mutant localised to the mitochondrial network when expressed together with SYTL5-EGFP in dKO cells (**Figure 2E**). Also, SYTL5-EGFP failed to localise to mitochondria in cells expressing RAB27A Q78L, further

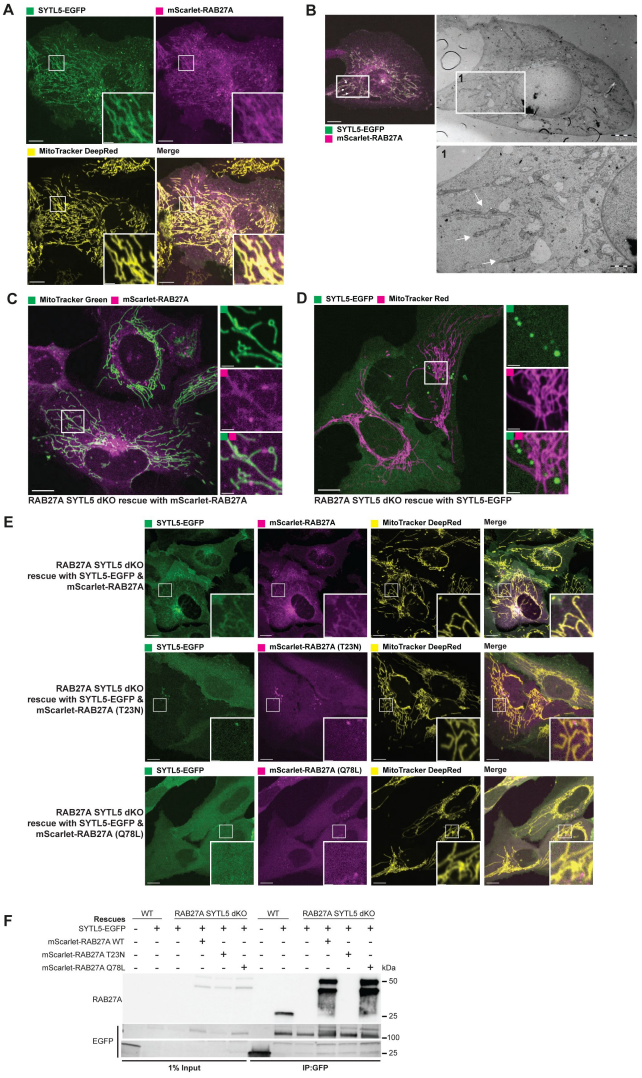

Figure 2.

Mitochondrial localisation of SYTL5 requires RAB27A GTPase activity

A. SYTL5-EGFP expression was induced for 24 h with 100 ng/ml doxycycline in U2OS cells with stable inducible expression of SYTL5-EGFP and constitutive expression of mScarlet-RAB27A. Cells were co-stained with MitoTracker DR for 30 min before live imaging. Arrows indicate mitochondrion filaments. Scale bars: 10 µm, 2 µm (insets).
B. CLEM analysis of the cells described in A. Before imaging, cells growing in monolayer were fixed in warm (≈37°C) 3.7% paraformaldehyde in 0.2 M HEPES (pH 7). After fixation, cells were imaged using a confocal microscope to acquire Z-stack of optical sections and DIC images to locate the cells of interest. The cells were finally fixed using 2% glutaraldehyde in 0.2 M HEPES (pH 7.4) for 120 min before sample preparation for TEM. Arrows in panel 1 indicate mitochondrion filaments. Scale bars: 15 µm (left), 5 µm (middle) and 2 µm (right).
C. U2OS dKO cells were rescued with mScarlet-RAB27A and co-stained with 50 nM MitoTracker green for 30 min before imaging. Scale bars: 10 µm, 2 µm (insets).
D. U2OS dKO cells were rescued with SYTL5-EGFP and co-stained with 50 nM MitoTracker red for 30 min before imaging. Scale bars: 10 µm, 2 µm (insets).
E. Live confocal microscopy imaging of U2OS dKO cells rescued with SYTL5-EGFP and mScarlet-RAB27A (upper panel); SYTL5-EGFP and mScarlet-RAB27A-T23N (middle panel) or SYTL5-EGFP and mScarlet-RAB27A-Q78L (lower panel). All cells were co-stained with 50 nM MitoTracker DR for 30 min before imaging. Scale bars: 10 µm, 2 µm (insets).
F. Lysates from U2OS cells stably expressing EGFP (control) and U2OS dKO cells expressing SYTL5-EGFP and/or mScarlet-RAB27A (wild-type, T23N or Q78L mutants) were immunoprecipitated using GFP-Trap beads and analysed by western blot using RAB27A and EGFP antibodies.

demonstrating that mitochondrial recruitment of SYTL5 depends on mitochondrial RAB27A localisation (**Figure 2E**). Taken together, our data indicate that the GTPase activity of RAB27A is required for its mitochondrial localisation, which facilitates further recruitment of SYTL5.

SYTL5 interacts with proteins involved in vesicle-mediated transport and cellular response to stress

As few molecular interactors of SYTL5 are known[1], we analysed the SYTL5 interactome by immunoprecipitating SYTL5-EGFP or an EGFP control, followed by mass spectrometry (MS) and protein-hit enrichment analysis. RAB27A was one of the most significant hits found, providing evidence that the IP was successful, together with several proteins known to participate in secretion such as PDCD6IP[27] (**Figure 3A**). In total, 163 proteins were identified as significant SYTL5-EGFP interactors compared to the EGFP control (**Figure 3A**, **Table 1**) and were subjected to Gene Ontology (GO) term enrichment analysis. Considering GO enrichment within the subcellular compartment ontology (GO-CC), we discovered the following compartments as enriched (**Figure 3B**) (number of hits for each category in parentheses): cytoskeleton (43), intracellular vesicle (38), extracellular vesicle (36), plasma membrane-bound cell projection (33), endosome (18) and focal adhesion (17). Furthermore, for biological processes, encoded in the GO-BP subontology, we discovered the following categories as enriched (**Figure 3A and C**): vesicle-mediated transport (38), cellular response to stress (34), response to oxygen-containing compound (31), intracellular protein transport (22), secretion (21), autophagy (13), stress-activated MAPK cascade (10), cellular response to oxidative stress (9), reactive oxygen species metabolic process (7), regulation of mitochondrion organization (6), endosome organization (4) and protein insertion into mitochondrial membrane (3). Taken together, the SYTL5 interactome implies a role for SYTL5 in mitochondrial processes and cellular response to stress, in line with its localisation to mitochondria, as well as a possible role in secretion and endocytosis, in line with its localisation to endocytic compartments and the plasma membrane (**Figure 1**).

SYTL5-RAB27A positive vesicles contain mitochondrial components

Several proteins involved in autophagy were identified as specific SYTL5 interactors, including SQSTM1/p62, ATG4B, TBK1, and ATP6V1A (**Figure 3A**), and given the mitochondrial localisation of SYTL5, we first investigated a possible role of SYTL5 in mitophagy. To induce mitophagy, dKO cells expressing mScarlet-RAB27A and SYTL5-EGFP were subjected to hypoxia or the drugs DFP (deferiprone, an iron chelator) or DMOG (Dimethyloxalylglycine, a prolyl-4-hydroxylase inhibitor) that mimics hypoxia by activation of HIF1α. We noticed an increase in the number and size of vesicles positive for SYTL5-EGFP and mScarlet-RAB27A that also contained MitoTracker Deep Red (MitoTracker DR) in all conditions, compared to control cells (**Figure 4A**).

HIF-1α is a transcription factor that is a main driver of the Warburg effect[15] and an inducer of mitophagy via upregulation of the outer mitochondrial membrane proteins BNIP3 and BNIP3L, which bind to LC3. To identify the nature of the SYTL5/RAB27A/MitoTracker DR positive vesicular structures that increase with HIF-1α stabilisation, dKO cells expressing mScarlet-RAB27A and SYTL5-EGFP were immunostained with antibodies against various autophagy markers. Intriguingly, while observing strong co-localisation of SYTL5/RAB27A/MitoTracker DR positive vesicles with LAMP1 (**Figure 4B**), the same structures did not co-localise with LC3B or the autophagy receptor p62 (**Supplementary Figure 4A**). However, as both LC3 and p62 are degraded in the lysosome, we added the lysosomal V-ATPase inhibitor Bafilomycin A1 (BafA1) for the last 4 hrs of DFP treatment, resulting in the presence of some LC3 and p62 positive SYTL5/RAB27A/MitoTracker DR vesicles (**Supplementary Figure 4B**). It should be noted that the SYTL5/RAB27A/MitoTracker-positive vesicle structures do not always colocalise with LAMP1, LC3 and p62, and that the phenotype of these cells is varied. The mitochondrial localisation of SYTL5 and RAB27A was not affected in cells treated with the ULK1 inhibitor MRT68291 or with the class III phosphoinositide 3-kinase VPS34 inhibitor IN1 (**Supplementary Figure 4C**), indicating that

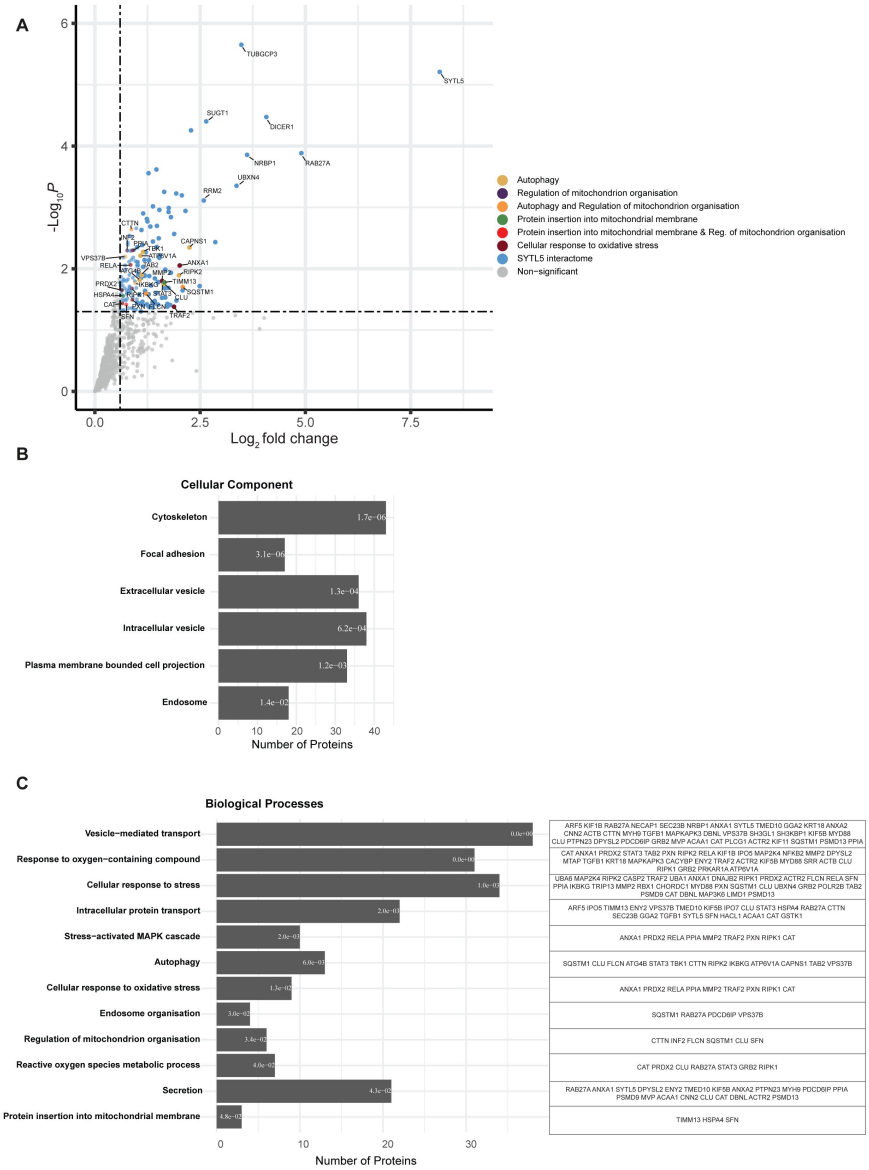

Figure 3.

SYTL5 interacts with proteins involved in vesicle-mediated transport and cellular response to stress

A. SYTL5 interactome. SYTL5-EGFP expression in U2OS cells was induced for 24 h using 100 ng/ml doxycycline, followed by immunoprecipitation of SYTL5-EGFP using GFP-Trap beads and identification of co-purified proteins by MS analysis. The list of co-purified proteins was compared with that obtained from cells expressing EGFP and only significant ($p<0.05$) SYTL5-EGFP specific protein hits are highlighted in colour. Protein hits falling into at least one of the biological processes; autophagy, regulation of mitochondrion organisation, protein insertion into mitochondrial membrane or cellular response to oxidative stress, are colour coded according to plot legend. All other significant hits are indicated in blue. Non-significant ($p>0.05$) are indicated in grey. Data are from 3 biological replicates.

B. GO cellular compartment term enrichment of significant protein hits co-purified with SYTL5-EGFP. Corresponding enrichment false discovery rate (FDR) value is represented inside each bar and bars are ordered from smallest to largest FDR (q-value) from top to bottom.

C. GO biological processes term enrichment of significant protein hits co-purified with SYTL5-EGFP.Corresponding enrichment FDR value is represented inside each bar and bars are ordered from smallest to largest FDR (q-value) from top to bottom. Proteins corresponding to each biological process category are listed in the table to the right.

Gene ID	logFC	P.Value	Protein ID
SYTL5	8,190967	6,18E-06	Q8TDW5
RAB27A	4,904658	0,00013	P51159; O00194
DICER1	4,072889	3,36E-05	Q9UPY3
NRBP1	3,616261	0,000139	Q9UHY1
TUBGCP3	3,480067	2,23E-06	Q96CW5
UBXN4	3,364929	0,000445	Q92575
PPME1	2,860594	0,003682	Q9Y570
SUGT1	2,644558	3,96E-05	Q9Y2Z0
RRM2	2,58741	0,000772	P31350
S100A16	2,489595	0,019199	Q96FQ6
RBX1	2,283705	5,54E-05	P62877
CAPNS1	2,245698	0,0045	P04632
IPO5	2,152529	0,001141	O00410
SQSTM1	2,087749	0,019914	Q13501
CDK5RAP1	2,083531	0,022579	Q96SZ6
PSMD9	2,066147	0,000637	O00233
ANXA1	2,015019	0,008846	P04083
RIPK2	1,998221	0,012785	O43353
TUBB2A	1,937802	0,032975	Q13885
FBXL18	1,932709	0,000593	Q96ME1
ACACA	1,884369	0,00271	Q13085; O00763
TRAF2	1,879215	0,041615	Q12933
ATXN10	1,807462	0,001441	Q9UBB4
PFKFB3	1,806392	0,011617	Q16875
CASC5	1,787295	0,038936	Q8NG31
ACTR2	1,753581	0,00102	P61160
PDCD6IP	1,750369	0,001188	Q8WUM4
DNAJB2	1,746104	0,020493	P25686
MTAP	1,723933	0,037343	Q13126
NOSIP	1,722576	0,041459	Q9Y314
LARP4	1,673434	0,010333	Q71RC2
ENY2	1,672969	0,029441	Q9NPA8
ARMCX3	1,661646	0,020894	Q9UH62
TIMM13	1,652287	0,016672	Q9Y5L4
ZC3HAV1L	1,646732	0,000559	Q96H79
CLU	1,641816	0,018032	P10909
STAT3	1,630662	0,017936	P40763
MMP2	1,596861	0,01583	P08253
ARHGAP28	1,594874	0,029771	Q9P2N2
CASP2	1,54764	0,006055	P42575

Table 1.

SYTL5 interactome

Proteins co-immunoprecipitated with SYTL5-EGFP vs EGFP expressing control.

NECAP1	1,532475	0,001098	Q8NC96; Q9NVZ3
CHORDC1	1,530842	0,006654	Q9UHD1
AHNAK2	1,518123	0,003188	Q8IVF2
P4HA2	1,507659	0,01657	O15460
SLAIN2	1,504025	0,038526	Q9P270
TTLL12	1,496256	0,016402	Q14166
CIAO1	1,47458	0,002001	O76071
PSMD13	1,469132	0,004425	Q9UNM6
PAPSS2	1,468267	0,024743	O95340
PKP3	1,462143	0,000241	Q9Y446
MAPKAPK3	1,43686	0,036615	Q16644
LAMC2	1,424905	0,014389	Q13753
TMED10	1,420889	0,033461	P49755
GGA2	1,401072	0,036446	Q9UJY4
SMYD5	1,380067	0,000962	Q6GMV2
MYD88	1,379573	0,0036	Q99836
PTPN23	1,372845	0,042911	Q9H3S7
PRMT3	1,367264	0,035439	O60678
SRR	1,335156	0,018756	Q9GZT4
METTL2B	1,318423	0,002052	Q6P1Q9
CEP55	1,303196	0,042401	Q53EZ4
KNTC1	1,293798	0,013151	P50748
MMADHC	1,287966	0,007304	Q9H3L0
RPS6KA4	1,278372	0,026028	O75676
TCEAL4	1,277767	0,041367	Q96EI5; Q9H3H9
KRT18	1,273972	0,000277	P05783
EIF3D	1,249965	0,001692	O15371
MAP3K6	1,235349	0,038163	O95382
FAM83D	1,235204	0,001544	Q9H4H8
FLCN	1,223376	0,025555	Q8NFG4
NARFL	1,207308	0,005387	Q9H6Q4; Q9UHQ1
TK1	1,191836	0,022913	P04183
TSN	1,182404	0,012781	Q15631
MOGS	1,181984	0,013095	Q13724
TRIP13	1,179669	0,007178	Q15645
SH3GL1	1,148087	0,001254	Q99961; Q99962
TGFB1	1,146935	0,009311	P01137
TBK1	1,146181	0,005314	Q9UHD2
UBAP2L	1,131475	0,034553	Q14157
HMMR	1,124677	0,038667	O75330
MAP2K4	1,123533	0,004105	P45985
LRRC40	1,116807	0,03566	Q9H9A6
TAB2	1,114102	0,012624	Q9NYJ8
IPO7	1,106622	0,002335	O95373
DECR1	1,096331	0,014198	Q16698
PRKAR1A	1,090646	0,049639	P10644

Table 1. (continued)

ATP6V1A	1,082598	0,006145	P38606
ATG4B	1,062937	0,01514	Q9Y4P1
CIAPIN1	1,056349	0,026294	Q6FI81
STIM1	1,036432	0,036684	Q13586
TSNAX	1,033898	0,012445	Q99598
PDLIM2	1,014087	0,008808	Q96JY6
KIF11	1,012826	0,007811	P52732
NCAPD2	1,005509	0,004454	Q15021
FLYWCH2	1,002772	0,036116	Q96CP2
FLNC	0,997402	0,031493	Q14315
ZCCHC11	0,995037	0,011036	Q5TAX3
ARF5	0,98277	0,002189	P84085; P61204; P18085; P84077
ARHGAP29	0,982689	0,020558	Q52LW3
INPP4A	0,977505	0,046529	Q96PE3
IKBKG	0,964638	0,017171	Q9Y6K9
CACYBP	0,96422	0,007507	Q9HB71
SEC23B	0,951773	0,047922	Q15437
CARHSP1	0,950642	0,016008	Q9Y2V2
STRN	0,93495	0,004936	O43815
KIAA0930	0,920553	0,044996	Q6ICG6
DPYSL3	0,910877	0,006555	Q14195
ACAA1	0,902484	0,014043	P09110
PPIA	0,901801	0,005015	P62937
JAK1	0,898744	0,029572	P23458
PXN	0,89135	0,032021	P49023
RIPK1	0,880408	0,02096	Q13546
HACL1	0,873144	0,005027	Q9UJ83
C16orf13	0,872785	0,043785	Q96S19
STAU2	0,871501	0,007129	Q9NUL3
CTTN	0,868965	0,002283	Q14247
NEDD1	0,865712	0,00298	Q8NHV4
RELA	0,848508	0,008652	Q04206
MOCS2	0,844002	0,02455	O96007
SESTD1	0,843323	0,022617	Q86VW0
CNN2	0,84227	0,005121	Q99439
TNS3	0,824331	0,019403	Q68CZ2; Q63HR2
MYH9	0,820463	0,020254	P35579; P35749
FAM120B	0,81995	0,012614	Q96EK7
PHLDB1	0,816857	0,002876	Q86UU1
LAMB3	0,811098	0,007705	Q13751
ERCC6L	0,809206	0,022191	Q2NKX8
RASA4	0,79333	0,044026	O43374; C9J798
SH3KBP1	0,78816	0,014872	Q96B97
ACTB	0,783173	0,00407	P60709; Q6S8J3; A5A3E0; P0CG38; Q562R1; P0CG39; Q9BYX7
CNN3	0,781781	0,003728	Q15417

Table 1. (continued)

DNMBP	0,770568	0,030522	Q6XZF7
INF2	0,769802	0,005056	Q27J81
NFKB2	0,762598	0,02469	Q00653
DOK1	0,758782	0,022414	Q99704
MVP	0,758137	0,025696	Q14764
SEPT9	0,750806	0,015745	Q9UHD8
SFN	0,747282	0,038485	P31947
UFSP2	0,736462	0,032911	Q9NUQ7
GNA13	0,729323	0,01046	Q14344
VPS37B	0,721343	0,006336	Q9H9H4
MCMBP	0,716545	0,008801	Q9BTE3
DPYSL2	0,707331	0,02086	Q16555
RNPEP	0,705101	0,032267	Q9H4A4
UBA6	0,691729	0,015468	A0AVT1
GSTK1	0,687332	0,046851	Q9Y2Q3
GMPS	0,683068	0,014906	P49915
POLR2B	0,676992	0,027717	P30876
DBNL	0,675429	0,006534	Q9UJU6
PLCG1	0,669824	0,049137	P19174
HSPA4	0,665847	0,027702	P34932
LIMD1	0,661786	0,018739	Q9UGP4
CAT	0,653596	0,036557	P04040
ANXA2	0,652983	0,016136	P07355; A6NMY6
CBR1	0,64346	0,032038	P16152; O75828
PRDX2	0,643131	0,022495	P32119
UBA1	0,634137	0,022102	P22314
NCAPG	0,632896	0,021943	Q9BPX3
MAT2A	0,622619	0,013543	P31153; Q00266
GRB2	0,619474	0,025687	P62993
KIF1B	0,612282	0,046537	O60333; Q12756; O43896
KIF5B	0,611182	0,018915	P33176; O60282; Q12840
MAT2B	0,602416	0,016771	Q9NZL9

Table 1. (continued)

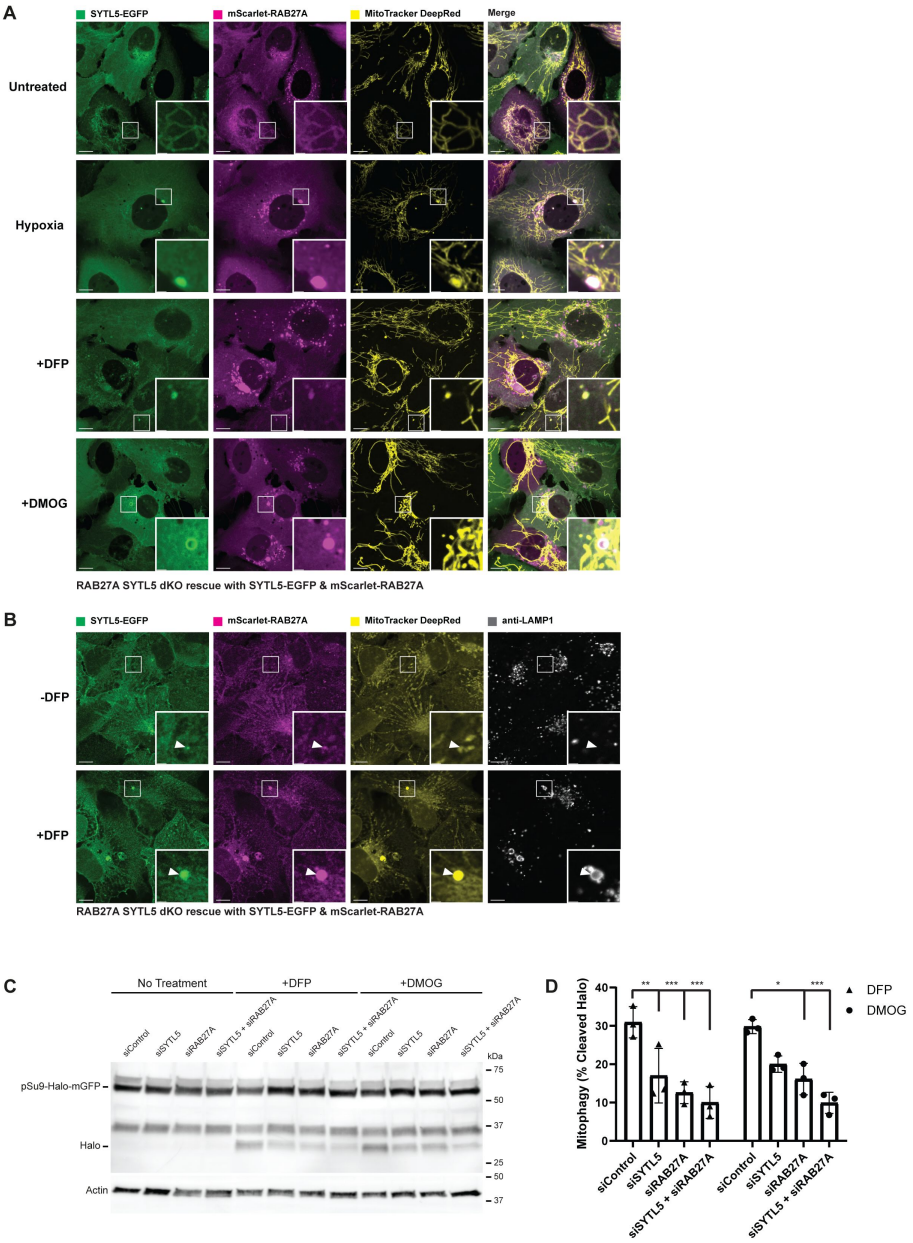

Figure 4.

Mitochondrial localisation of SYTL5 and RAB27A is not perturbed by autophagy inhibition or mitophagy stimulation

A. SYTL5/RAB27A dKO U2OS cells rescued with SYTL5-EGFP and mScarlet-RAB27A were untreated (upper panel) or treated with 1 mM DFP (2nd panel), hypoxia (1% O_2) (3rd panel) or 1 mM DMOG (4th panel) for 24 h. All cells were stained with 50 nM MitoTracker DR 30 min prior to live confocal microscopy imaging. Scale bars: 10 µm, 2 µm (insets).
B. SYTL5/RAB27A dKO U2OS cells rescued with SYTL5-EGFP and mScarlet-RAB27A were treated or not with 1 mM DFP for 24 h. Cells were stained with 50 nM MitoTracker DR prior to fixation. Fixed cells were stained with a LAMP1 antibody and imaged by confocal microscopy. Scale bars: 10 µm, 2 µm (insets). Arrowheads point to SYTL5/RAB27A-positive structures.
C. U2OS cells expressing pSu9-Halo-mGFP were transfected with 20 nM control siRNA, SYTL5 siRNA #1 or RAB27A siRNA #1 for 48 h before 20 min incubation with the TMR-conjugated Halo ligand followed by 24 h incubation with 1 mM DFP or 1 mM DMOG. Cell lysates were analysed by western blot for the Halo tag. Actin was used as a loading control.
D. Quantification of data in C. Error bars represent the mean with standard deviation between replicates (n=3). Significance was determined by two-way ANOVA followed by Tukey's multiple comparison test. * = p< 0.05, ** =p< 0.01, *** = p<0.001.

SYTL5 and RAB27A are recruited to mitochondria independent of active autophagy. Thus, our data show that SYTL5 and RAB27A-positive vesicles containing mitochondrial material and autophagic proteins form upon HIF-1α induced mitophagy.

SYTL5 and RAB27A function as positive regulators of selective mitophagy

To investigate whether SYTL5 and RAB27A are required for the turnover of mitochondrial proteins in hypoxic conditions, we took advantage of two mitophagy reporter U2OS cell lines, one expressing the mitochondrial matrix reporter, pSu9-Halo-mGFP[28] and one expressing the mitochondrial targeting signal of the matrix protein NIPSNAP1 tagged with EGFP-mCherry[29] (hereafter referred to as IMLS cells).

The pSu9-Halo-mGFP cells allow a measure of mitophagy flux via the production of a cleaved Halo Tag band, which is stable in lysosomes when bound to the ligand ($Halo^{TMR}$). Activation of HIF1α by treatment with DFP or DMOG resulted in the appearance of cleaved $Halo^{TMR}$ (**Figure 4C-D**) consistent with activation of mitophagy. The use of small interfering RNA (siRNA) to deplete SYTL5, RAB27A or both simultaneously in these cells, resulted in a significant reduction in the amount of free $Halo^{TMR}$ (**Figure 4C-D**) highlighting a reduction in mitophagy. Depletion of SYTL5 and/or RAB27A did not affect the DFP or DMOG-induced HIF1α activation, as analysed by BNIP3L expression levels (**Supplementary Figure 5A**). Thus, both SYTL5 and RAB27A are required for the lysosomal turnover of mitochondrial components in response to HIF1α activation and not for the HIF1α mediated induction of mitophagy.

In contrast, we did not observe a significant difference in mitophagy levels in IMLS cells depleted of SYTL5 or RAB27A treated with DFP to induce Parkin-independent mitophagy, or in IMLS cells with stable expression of Parkin treated with the uncoupler carbonyl cyanide m-chlorophenyl hydrazone (CCCP) to induce Parkin-dependent mitophagy (**Supplementary Figure 5B-E**), together indicating that macro-mitophagy proceeds independently of SYTL5 and RAB27A. In line with this, the starvation-induced autophagic flux was not affected in cells lacking SYTL5 (**Supplementary Figure 5F**).

Taken together, our results indicate that SYTL5 and RAB27A function to regulate the lysosomal turnover of selected mitochondrial proteins in response to hypoxic conditions.

SYTL5 regulates mitochondrial respiration

Our finding of mitochondrial material within SYTL5-RAB27A positive structures upon induction of mitochondrial stress through DFP and hypoxia (**Figure 4A**), together with reduced turnover of the Fo-ATPase subunit 9 upon knockdown of SYTL5 and RAB27A (**Figure 4C-D**) and the identification of several proteins involved in the cellular response to stress (**Figure 3C**), including mitochondrial proteins (e.g., DECR1 and TIMM13), in the SYTL5 interactome (**Figure 3A**) led us to investigate a potential role of SYTL5 and RAB27A in mitochondrial function and bioenergetics.

The cellular oxygen consumption rate (OCR) can be measured with the Seahorse analyser upon sequential addition of different inhibitors (oligomycin, CCCP, antimycin and rotenone) that block the function of specific electron transport chain (ETC) complexes[30]. SYTL5 KO cells had a significant decrease in both basal and ATP-linked respiration compared to WT U2OS cells (**Figure 5A-B**), indicating reduced mitochondrial OXPHOS activity. As for RAB27A, both basal respiration and ATP-linked OCR were significantly reduced in cells depleted of RAB27A (RAB27A KO and RAB27A/SYTL5 dKO) relative to the control (**Figure 5A-B**), indicating an important function of these proteins in regulation of mitochondrial respiration.

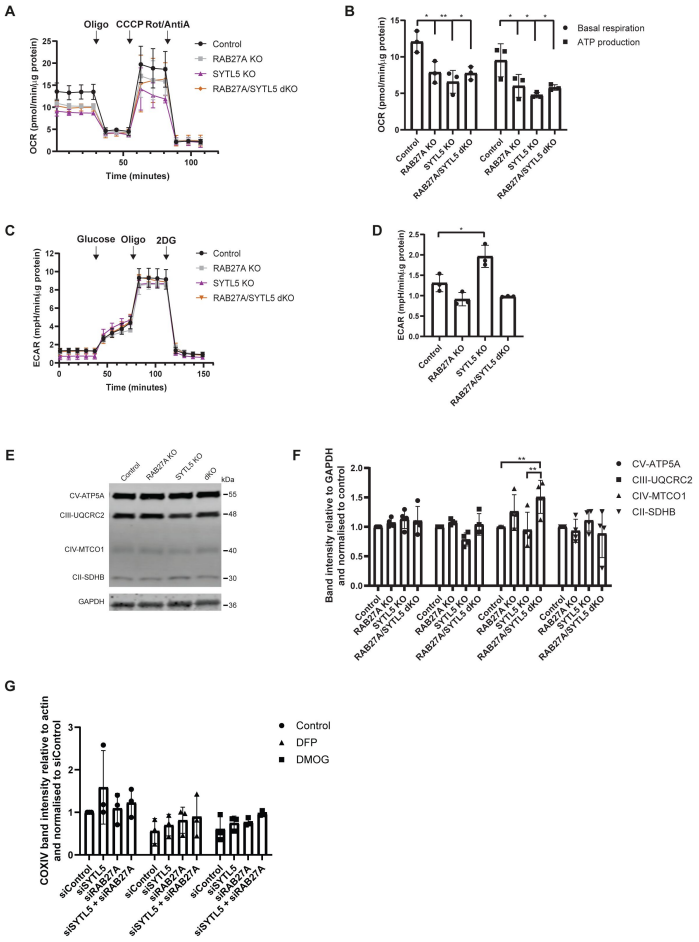

Figure 5.

SYTL5 and RAB27A regulate mitochondrial bioenergetics.

A. Mitochondrial oxygen consumption rate was analysed in U2OS control cells, SYTL5 KO, RAB27A KO and dKO cells using the Seahorse XF analyser. OCR was measured after sequential addition of oligomycin, CCCP and a combination of rotenone and antimycin-A into the assay medium. Error bars represent the mean with standard deviation between replicates (n=3).
B. The four basal OCR measurements per well (before oligomycin addition) were averaged to obtain the basal OCR value and the non-mitochondrial respiration was subtracted to determine the basal respiration associated to each condition. The ATP production was calculated by subtracting the proton leak from the maximal respiratory capacity. Error bars represent the mean with standard deviation between replicates (n=3). Significance was determined by two-way ANOVA followed by Bonferroni multiple comparison test, * = p< 0.05, ** = p<0.01.
C. The extracellular acidification rate (ECAR) was analysed in U2OS control cells, SYTL5 KO, RAB27A KO and dKO cells using the Seahorse XF analyser. ECAR was measured upon addition of glucose, oligomycin and 2-DG using control and SYTL5 depleted cells. Error bars represent the mean with standard deviation between replicates (n=3).
D. The glycolysis rate of each condition was calculated by subtracting the ECAR value after 2-DG treatment to the ECAR after addition of glucose (Glycolysis=ECAR after addition of glucose−ECAR after 2-DG treatment). Error bars represent the mean with standard deviation between replicates (n=3). Significance was determined by one-way ANOVA followed by Tukey multiple comparison test, * = p< 0.05.
E. Cell lysates from U2OS control, RAB27A KO, SYTL5 KO and dKO cells were analysed by western blot for the indicated electron transport chain complex-II, -III, -V and -V proteins. GAPDH was used as a loading control.
F. Quantification of data in E. Band intensities were quantified relative to GAPDH and normalised to control. Error bars represent the mean with standard deviation between replicates (n=4). Significance was determined by two-way ANOVA followed by Bonferroni multiple comparison test, ** = p<0.01.
G. U2OS cells were transfected with 20 nM control siRNA, SYTL5 siRNA #1 or RAB27A siRNA #1 for 48 h followed by 24 h incubation with 1 mM DFP or 1 mM DMOG. Cell lysates were analysed by western blot for COXIV. Actin was used as a loading control. Error bars represent the mean with standard deviation between replicates (n=3).

To test whether the decreased respiration in cells depleted of SYTL5 and/or RAB27A is coupled to a shift to glycolysis, we performed Seahorse analysis of the extracellular acidification rate (ECAR) in cells upon the sequential addition of glucose (increases glycolytic capacity), oligomycin (inhibits mitochondrial ATP production), and 2-DG (a glycolysis inhibitor which causes an abrupt decrease in ECAR). Intriguingly, glycolysis was significantly increased in SYTL5 KO cells as compared to control (**Figure 5C-D**), indicating a possible metabolic shift to compensate for the decrease in OCR observed when SYTL5 was depleted (**Figure 5A-B**). In contrast, ECAR was reduced in cells lacking RAB27A compared to the control, which may indicate an impairment in glucose uptake (**Figure 5C**) and therefore in glycolysis (**Figure 5D**). After adding oligomycin the ECAR increased in all cell lines, but in RAB27A KO and dKO cell lines, the increase was reduced when compared to the control cell line (**Figure 5C-D**).

The clear reduction in mitochondrial respiration observed in cells lacking RAB27A and SYTL5 led us to investigate the abundance of various ETC proteins. Depletion of SYTL5 and/or RAB27A did not affect the overall abundance of ATP5A (complex V), UQCRC2 (complex III) or SDHB (complex II), but we observed a significant increase in the level of MTCO1 (complex IV) in cells lacking RAB27A (**Figure 5E-F**). There was however no significant difference in the level of COXIV, another subunit of the ETC complex IV, upon siRNA-mediated knockdown of SYTL5, RAB27A or both compared to siControl in basal condition or upon induction of mitophagy with DFP or DMOG (**Figure 5G**).

Taken together, our data show that both RAB27A and SYTL5 are important for normal mitochondrial respiration and ATP production while SYTL5 seems to regulate a metabolic switch to glycolysis.

Low SYTL5 expression is related to reduced survival for adrenocortical carcinoma patients

Since our data indicate that SYTL5 may be a regulator of the metabolic switch from oxidative phosphorylation to glycolysis (the Warburg effect) (**Figure 5A-D**) that is frequently associated with cancer cells, we decided to analyse publicly available expression datasets to explore a possible link between SYTL5 and cancer. Using bulk RNA expression data from healthy/normal tissue samples in the GTEx project, we found that SYTL5 is preferentially expressed in adrenal gland and various regions of the brain (**Figure 6A**). Adrenocortical carcinoma (ACC) is a rare type of aggressive cancer with poor prognosis and limited treatment options that develops in the adrenal cortex[23]. A comparison of gene expression levels[31] in normal adrenal gland samples and ACC samples showed that SYTL5 mRNA expression is significantly reduced in tumour samples. (**Figure 6B**). Furthermore, patient survival analysis using data obtained from the TCGA-ACC cohort, indicates that low SYTL5 mRNA expression is associated with a significantly reduced survival of ACC patients (**Figure 6C**), suggesting a possible tumour suppressor function for SYTL5 in ACC cancer progression. RAB27A expression levels were also reduced in tumor tissue compared to normal samples, although to a lesser extent than SYTL5 (**Figure 6D**), and overall patient survival in ACC patients did not show any relationship with RAB27A expression levels (**Figure 6E**).

The adrenal gland cortex secretes several steroid hormones, such as mineralocorticoids (e.g. aldosterone), glucocorticoids (e.g. cortisol), and adrenal androgens (DHEA and DHEA-sulphate)[32], to the bloodstream. ACC tumours are characterised by excess adrenocortical hormone production in nearly 45–70% of patients, with hypercortisolism being the most common[23]. As mitochondria contain enzymes essential for steroid hormone biosynthesis from cholesterol[24], we asked whether SYTL5 may regulate cortisol production. SYTL5 or RAB27A were depleted by siRNA in the ACC cell line H295R, followed by quantification of cortisol secretion using a colorimetric assay. We did not observe a significant change in cortisol secretion upon SYTL5 or

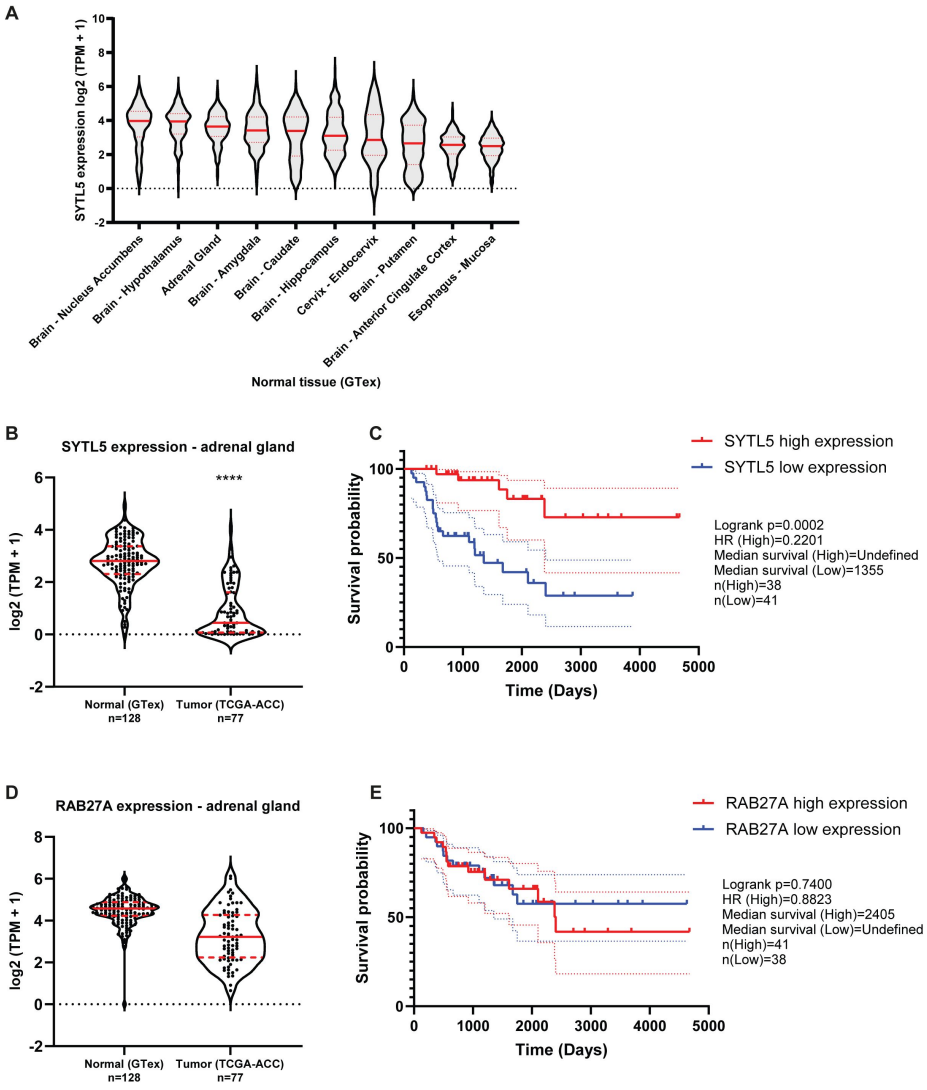

Figure 6.

Low SYTL5 expression is related to reduced survival for adrenocortical carcinoma patients.

A. SYTL5 expression levels in normal/healthy tissues, using data from the GTEx project (v8). Shown are the 10 tissue sites for which SYTL5 is most highly expressed (i.e. based on median expression levels). TPM = transcripts per million. Median is represented by a red solid line and quartiles by red dashed lines.
B. Comparison of SYTL5 gene expression levels in normal adrenal gland samples (GTEx, n = 128) and adrenocortical carcinoma samples (The Cancer Genome Atlas (TCGA) ACC cohort, n = 77). Median expression is represented by a red solid line and quartiles by red dashed lines. Statistical analysis was performed using the unpaired t-test with Welch's correction. TPM= transcripts per million.
C. Kaplan-Meier plot for ACC patient survival related to SYTL5 expression levels. The events related to high SYTL5 expression (expression level above median) are indicated in red and the dotted lines represent 95% confidence interval. Events related to low SYTL5 expression (expression level below median) are indicated in blue and the dotted lines represent 95% confidence interval. Statistical analysis was performed using Logrank (Mantel-Cox) test.
D. Comparison of RAB27A gene expression levels in normal adrenal gland samples (GTEx, n = 128) and adrenocortical carcinoma samples (The Cancer Genome Atlas (TCGA) ACC cohort, n = 77). Median expression is represented by a red solid line and quartiles by red dashed lines. Statistical analysis was performed using the unpaired t-test with Welch's correction.
E. Kaplan-Meier plot for ACC patient survival related to RAB27A expression levels. The events related to high RAB27A expression (expression level above median) are indicated in red and the dotted lines represent 95% confidence interval. Events related to low RAB27A expression (expression level below median) are indicated in blue and the dotted lines represent 95% confidence interval. Statistical analysis was performed using Logrank (Mantel-Cox) test.

RAB27A knockdown (**Supplementary Figure 6**), indicating that the correlation between low SYTL5 expression levels and ACC patient survival likely is unrelated to effects on cortisol production.

Discussion

SYTL5 has been identified as a RAB27A effector protein with affinity for membranes through its C2 lipid-binding domains[1], but nothing is known about a potential role of SYTL5 in regulation of RAB27A-dependent membrane trafficking pathways. Using the osteosarcoma derived U2OS cell line, here we confirm that SYTL5 interacts with RAB27A, and show that it localises to mitochondria and small, highly mobile vesicles interacting with the mitochondrial network, as well as to endolysosomal and endocytic compartments, indicating a role of SYTL5 in cellular membrane trafficking events.

Most interestingly, mitochondrial recruitment of SYTL5 involves coincidence detection, as it requires both its RAB27-binding SHD domain and its lipid-binding C2 domains. Indeed, we demonstrate that SYTL5 is recruited to mitochondria in a RAB27A-dependent manner and that RAB27A itself is localised to mitochondria in a manner dependent on its GTPase activity, as both RAB27A GDP and GTP mutants (T23N and Q78L, respectively) showed a dispersed cytoplasmic localisation. This is in line with a study showing that the GTPase activity of RAB27A is required for its localisation to melanosomes[33]. The mechanisms involved in mitochondrial recruitment of RAB27A are not clear. It is however interesting to note that other RAB proteins are recruited to the mitochondria by regulation of their GTPase activity. During parkin-mediated mitophagy, RABGEF1 (a guanine nucleotide exchange factor) is recruited through its ubiquitin-binding domain and directs mitochondrial localisation of RAB5, which subsequently leads to recruitment of RAB7 by the MON1/CCZ1 GEF complex[34]. Intriguingly, ubiquitination of the RAB27A GTPase activating protein alpha (RAB27B) is reduced in the brain of Parkin KO mouse compared to controls[35], suggesting a possible connection of RAB27A with regulatory mechanisms that are linked with mitochondrial damage and dysfunction.

SYTL5 and RAB27A are both members of protein families, suggesting possible functional redundancies from Rab27B or one of the other SYTL isoforms. While RAB27B has a very low expression in U2OS cells, all five SYTL's are expressed. However, when knocking out or knocking down SYTL5 and RAB27A we observe significant effects that we presume would be negated if their isoforms were providing functional redundancies. Moreover, we did not detect any other SYTL protein or RAB27B in the SYTL5 interactome, confirming that they do not form a complex with SYTL5.

Given the presence of mitochondria-associated small and highly mobile SYTL5/RAB27A-positive vesicles that contain mitochondrial material and stain positive for LAMP1, we speculate that RAB27A and SYTL5 facilitate mitophagy-mediated lysosomal delivery of mitochondria or selected mitochondrial components. Indeed, SYTL5 and RAB27A positive vesicles containing mitochondrial material were observed in cells upon hypoxia or hypoxia-mimicking (DFP and DMOG) treatments, where some vesicles stained positive for the autophagy markers p62 and LC3B upon co-treatment with the lysosomal V-ATPase inhibitor BafA1. Intriguingly, in cells treated with DFP and DMOG we observed a significant decrease in lysosomal cleavage of the mitophagy reporter pSu9-Halo-mGFP[36] upon depletion of SYTL5 and/or RAB27A. Additionally, when blotting for various endogenous proteins of the electron transport chain complexes, we found that the level of the cytochrome c oxidase (complex IV) subunit MTCO1/COX1 was significantly increased in cells lacking RAB27A. However, neither the basal level of COXIV, another complex IV subunit, nor the lysosomal targeting of a mitochondrial matrix reporter (IMLS) were affected by depletion of SYTL5 and/or RAB27A. Expression of the mitophagy receptor BNIP3L, a HIF-1a target, was not affected by SYTL5 and/or RAB27A depletion. Mitochondrial recruitment of SYTL5 and RAB27A was also

independent of the core autophagy machinery components ULK1 and VPS34. Taken together, our data indicate that mitochondrial RAB27A/SYTL5 function as positive regulators of selective clearance of mitochondrial components, in a piece-meal mitophagy-dependent manner.

The role of SYTL5 and RAB27A in the turnover of proteins involved in mitochondrial oxidative phosphorylation and ATP production is reminiscent of the recently described VDIM (Vesicles Derived from the Inner Mitochondrial membrane) pathway[16]. VDIMs are formed by IMM herniation through pores in the outer mitochondrial membrane, followed by their engulfment by lysosomes in proximity to mitochondria in a process that is independent of the core autophagy machinery. However, in contrast to our findings, VDIMs lack LC3 and p62 and oxidative stress-induced VDIM formation leads to selective degradation of IMM proteins, including COX4.

Mitochondria are known stress sensors and hubs for cellular adaptation[8]. When analysing the interactome of SYTL5, we found that many candidates were related to the cellular response to stress and oxygen-containing compounds, as well as vesicle-mediated transport and secretion. In line with a role for SYTL5/RAB27A in the regulation of mitochondrial stress, we found that cells lacking SYTL5 and/or RAB27A displayed reduced OXPHOS activity and ATP-production. A shift from OXPHOS to anaerobic glycolysis occurs in normal cells during hypoxic conditions and often in cancer cells even under normoxic conditions, commonly referred to as the Warburg effect[22]. Intriguingly, while the depletion of SYTL5 triggered a shift to glycolysis as observed by an increase in the extracellular acidification rate (ECAR) due to cellular lactate production, depletion of RAB27A or both RAB27A/SYTL5 had no significant effect, indicating that SYTL5 may function as a negative regulator of RAB27A and subsequently the Warburg effect.

The observed switch from OXPHOS to glycolysis in U2OS cells depleted of SYTL5 prompted us to look at cancer patient databases. We observed, using data from GTEx, that the adrenal gland is among the tissues with highest levels of SYTL5 gene expression, and that its expression is reduced in adrenocortical carcinoma samples (TCGA-ACC) when compared to normal adrenal gland tissue. Moreover, low SYTL5 expression is associated with reduced ACC patient survival. One characteristic of this type of cancer is an increase in steroid hormone production and secretion. Most steroid hormones are produced in mitochondria[24] but we did not observe any changes in the level of cortisol in ACC cells depleted of SYTL5. The mechanisms linking SYTL5 to the Warburg effect and ACC need further investigation, but it is interesting to note that RAB27A expression levels do not correlate with ACC survival.

To summarise, we show that SYTL5 is a RAB27A effector protein being recruited to mitochondria in a RAB27A-dependent manner. Upon hypoxia, RAB27A and SYTL5 promote lysosomal clearance of selected mitochondrial components, and both proteins are needed for mitochondrial respiration. We identify SYTL5 as a negative regulator of the Warburg effect and potentially tumorigenesis.

Materials and methods

Antibodies and dyes

Antibody	Source	Identifier
α-Tubulin	Sigma-Aldrich	#T5168
β-Actin	Cell signalling technology	#3700
BNIP3L	Cell signalling technology	#12396
COXIV	Cell signalling technology	#4850
EGFP	Abcam; Clontech	#ab290; #632569
FLAG Tag	Cell signalling technology	#14793
GAPDH	Cell signalling technology	#5174
Halo Tag	Promega	#G9211
LAMP1	Santa Cruz Biotechnology	#sc-20011
LC3	MBL international	#PM036
OXPHOS	Abcam	#ab110413
p62	Progen	#GP62-C
RAB27A	Santa Cruz Biotechnology	#sc-74586
SYTL5	Sigma-Aldrich	#HPA026074
TIM23	BD biosciences	#611223
TOMM20	Santa Cruz Biotechnology	#sc-17764
LysoTracker red DND-99	ThermoFisher Scientific	#L7528
MitoTracker™ Deep Red FM	ThermoFisher Scientific	# M22426
MitoTracker™ Green FM	ThermoFisher Scientific	#M7514
MitoTracker™ Red CMXRos	ThermoFisher Scientific	#M7512

Cell culture, lentivirus production and stable cell line generation

Human bone osteosarcoma epithelial cells (U2OS FlpIn TRex cell line, kindly provided by Steve Blacklow, Harvard Medical School, US) were grown in complete medium of Dulbeccós Modified Eagle Medium (DMEM; Lonza #12-604F and Gibco # 31966047) with 10% v/v foetal bovine serum (FBS; Sigma-Aldrich #F7524),100 U/ml Penicillin and 100 µg/ml Streptomycin (P/S; Thermo Fisher Scientific #15140122) at 37 °C with 5% CO2.

For lentiviral particle production HeK-FT cells were co-transfected with 1.6 µg of pLVX lentiviral vector, pCMV-VSV-G and psPAX2 using X-tremeGENE™ 9 DNA Transfection Reagent (Sigma #XTG9-RO). For virus infection, cells were seeded in complete medium and supplemented with 8 µg/ml polybrene (Santa Cruz Biotechnology #sc-134220). 2 µg/ml Puromycin (Sigma Aldrich #P7255) was added after 24 h post-infection for selection. To generate U2OS stably expressing SYTL5-EGFP, U2OS FlpIn TRex cells and U2OS FlpIn TRex_mScarlet-RAB27A were co-transfected with 0.1 µg pcDNA™5/FRT/TO_SYTL5-EGFP and 0.9 µg pOG44 Flp recombinase expression vector using Lipofectamine™ 2000 (Thermo Fisher Scientific #11668019) according to the manufacture's instructions. To produce stable cell lines expressing pLVX-SV40-mScarlet-RAB27A(T23N/Q78L) and pLVX-CMV-SYTL5-EGFP-3xHA, U2OS dKO cells were infected with lentiviral particles followed by

fluorescence-activated cell sorting (FACS) for double mScarlet/EGFP expressing cells. To generate stable cells expressing pLVX-CMV-SYTL5-EGFP-3xFLAG, pLVX-CMV-SYTL5 (ΔC2AB)-EGFP-3xFLAG and pLVX-CMV-SYTL5 (ΔSHD)-EGFP-3xFLAG, U2OS FlpIn TRex cells were infected with lentiviral particles. To generate U2OS stably expressing pSu9-Halo-mGFP, U2OS cells were infected with retroviral particles generated using pUMVC (addgene # 8449) and pMRX-IB-pSu9-HaloTag7-mGFP (addgene # 184905). Stable cell lines were maintained in complete medium with additional 5 µg/ml blasticidin S (Thermo Fisher Scientific #R21001) or 2 µg/ml puromycin (Sigma Aldrich #P7255). For starvation experiments, cells were washed with PBS and incubated for 4 h in Earlés balanced salt solution (EBSS; Gibco #24010043).

NCI-H295R cells were obtained from ATCC (#CRL-2128) and maintained in DMEM: F12, HEPES medium (Gibco #11330032) supplemented with 2.5% Nu-Serum (Corning #355100), 1% ITS+Premix Universal culture supplement (Corning #354352) and 100 µg/ml P/S (Thermo Fisher Scientific #15140122) at 37 °C with 5% CO2.

Hypoxia and drug treatments

After cells were seeded, they were transferred to a INVIVO$_2$ 200 Hypoxic workstation (Ruskinn). Hypoxia treatment was carried out for 24 hours with oxygen concentration set to 1%.

Drugs were added into the cell media. Treatment durations and drug concentrations are indicated in the figure legends. Drugs used were DFP (Sigma-Aldrich #379409), DMOG (Sigma-Aldrich #D3695), VPS34IN1 (Selleckchem # S7980) and MRT68291 (Selleckchem #S7949).

Molecular cloning

SYTL5 was amplified from WT U2OS cDNA (5'-ATGTCTAAGAACTCAGAGTTCATC-3' and 5'-TTAGAGCCTACATTTTCCCATG-3') and cloned into Zero Blunt TOPO vector using Zero Blunt™ TOPO™ PCR Cloning Kit (Thermo Fisher Scientific #450245) according to the manufacture's instructions. pcDNA™5/FRT/TO_SYTL5-EGFP was generated by Gibson Assembly using the TOPO-SYTL5 vector as a template for SYTL5 and cloned into a pcDNA™5/FRT Mammalian Expression Vector (Thermo Fisher Scientific #V601020) or into a pLVX-CMV lentiviral expression vector. Truncated SYTL5 (ΔSHD) and SYTL5 (ΔC2AB) were generated by Gibson assembly using the pcDNA™5/FRT/TO_SYTL5-EGFP construct as a template and cloned into a pLVX-CMV lentiviral expression vector.

RAB27A was amplified from WT U2OS cDNA and cloned into a pLVX-SV40 lentiviral expression vector. RAB27A mutations were performed using the site-directed mutagenesis QuikChange II kit (Agilent #200524) according to the manufacture's instructions using the following primer pairs:

Mutation	Forward primer	Reverse primer
RAB27A_T23N (c68a)	atattggtaaagtacactgttcttccctacaccagagtc	gactctggtgtagggaagaacagtgtactttaccaatat
RAB27A_Q78L (a233t)	tacgaaacctctccagccctgctgtgtcc	ggacacagcagggctggagaggtttcgta

CRISPR knockout cell line generation and validation

SYTL5 and RAB27A gene knockouts were performed as previously described by Ran *et al*., 2013. Briefly, gRNA target sequences were designed using Wellcome Sanger Institute Genome Editing (WGE) design tool available at *https://wge.stemcell.sanger.ac.uk/find_crisprs*.

Target gene	gRNA sequence	Genomic location
RAB27A	AGTGGCTCCATCCGGCCCAC	chr15:55230454
SYTL5 guide 1	CGACTAATACTTGCCAGAGC	chrX:38034292
SYTL5 guide 2	ATACGTAGAACAGCCTCCAC	chrX:38033693

DNA oligos were annealed and phosphorylated before cloning into pSpCas9(BB)-2A-Puro (PX459) V2.0 (addgene # 62988). The obtained CRISPR plasmids were transfected into U2OS Flp-In TRex cells using Lipofectamine™ 2000 according to the manufacture's instructions and selection with 2 µg/ml puromycin (Sigma Aldrich #P7255) was applied for 24 h. Limiting dilutions were performed using a concentration of 15 cells/ml and seeded in complete medium in a 384 well plate. Single colonies were collected ~10 days after seeding and expanded for a further 3 weeks. For genotyping, gDNA from each single clone line was isolated using QIAamp DNA Mini Kit (QIAGEN #51304) and the targeted genomic region was amplified by PCR using flanking primers (RAB27A: 5'-ATAACCTCTCCCTTGACCTTGTATG-3' and 5'-TAGATGCCTTTGGGATTTGTACTGA-3'; SYTL5: 5'-CAGGTCCCTTTCTTCTCGCA-3' and 5'-TCAGTCAGCTGCAAGAGTGG-3'). The PCR product was cloned into Zero Blunt TOPO vector using Zero Blunt™ TOPO™ PCR Cloning Kit according to the manufacture's instructions. RAB27A clonal lines were validated by western blot, and SYTL5 deletions were detected by running PCR products in 1% w/v agarose gel (Thermo Fisher Scientific #R2801).

siRNA knockdown by reverse transfection

For siRNA knockdown, cells were incubated with OptiMEM (Thermo Fisher Scientific # 31985047) and Lipofectamine RNAiMAX (Thermo Fisher Scientific #13778150) for 5 min at room temperature (RT). Followed by addition of 20 nM siRNA diluted in OptiMEM and 15 min incubation at RT. Cells were fixed/harvested after 72 h of knockdown. The siRNA used for mRNA depletion are the following: siControl: 5'-UAACGACGCGACGACGUAAtt-3'; siSYTL5 #1: 5'-CUCUUAGAAGCAAAACGUAtt-3'; siSYTL5 #2: 5'-CAACAAGCGUAAGACCAAAtt-3'; siSYTL5 #3: 5'-GGUUUGUGCUUCAACCCAAtt-3'; siRAB27A #1: 5'-GGAAGACCAGUGUACUUUAtt-3' and siRAB27A #2: 5'-CCAGUGUACUUUACCAAUAtt-3'.

RNA isolation, cDNA synthesis and RT-PCR

RNA was isolated using TRIzol reagent (Thermo Fisher Scientific #15596026) and cDNA was synthesised using SuperScript III Reverse Transcriptase (Thermo Fisher Scientific #18080085) according to the manufacture's instructions. qPCR analysis was performed using KAPA SYBR FAST qPCR Kit (Sigma-Aldrich #KK4601) and relative mRNA expression levels were normalised to the expression levels of TATA-binding protein (TBP) using the comparative ΔCt method. The primers used were the following:

SYTL5: 5'-GTGACAAAATCGCGCAGCTA-3', 5'-GGACAACATCAGTGCCGAGA-3'

RAB27A: 5'-GGAGAGGTTTCGTAGCTTAACG-3', 5'-CCACACAGCACTATATCTGGGT-3'

TBP: 5'-CAGAAAGTTCATCCTCTGGGCT-3', 5'-TATATTCGGCGTTTCGGGCA-3'

Immunofluorescent staining

Cells were fixed in 4% paraformaldehyde (PFA) (Sigma-Aldrich #158127) in PBS for at least 15min at 37°C, quenched for 10 min using 0.05 M NH4Cl in PBS, permeabilised in 0.05% saponin in PBS for 5 min and blocked in 1% BSA in PBS for 30 min at room temperature. Antibody staining was

performed in a wet chamber for 1 h at room temperature and the antibodies were diluted in PBS containing 0.05% saponin. Nuclei staining was performed using Hoechst 33342 (Thermo Fisher Scientific #H1399) diluted in PBS at 1µg/ml.

Light microscopy

Cells expressing inducible fluorescent proteins were induced with 100 ng/ml doxycycline (Clontech #631311) for 24 h. For live cell confocal microscopy cells were incubated with indicated dyes prior to imaging. Imaging was carried out with either the Andor Dragonfly High Speed Confocal Microscope or the Nikon Crest V3 with a 60x oil immersion objective (NA 1.4). High content widefield imaging was conducted with the ImageXpress Micro Confocal (Molecular Devices) microscope with a 20x objective (NA 0.45). Fixed immunofluorescence confocal imaging was performed using the Andor Dragonfly High Speed Confocal Microscope or Nikon Crest V3 both with a 60x oil immersion objective (NA 1.4) or Zeiss LSM 800 microscope (Zen Black 524 2012 SP5 FP3, Zeiss) with a 63x oil immersion objective (NA 1.4).

Correlative light electron microscopy

U2OS cells co-expressing SYTL5-EGFP and mScarlet-RAB27A were seeded in gridded glass-bottom cell culture dishes (MatTek #P35G-1.5-14-CGRD). Cells growing in monolayer were fixed in warm (≈37°C) 3.7% PFA in 0.2 M HEPES (pH 7) and imaged using the Andor Dragonfly High Speed Confocal Microscope. After imaging, the samples were fixed using 2% v/v glutaraldehyde in 0.2 M HEPES, pH 7.4. After post-fixation in 2% v/v osmium tetraoxide and 3% v/v K4[Fe(CN)6], samples were embedded in Epon and 60 nm thickness sections were cut with a diamond knife. Sections were analysed using a JEM-1400 Plus Transmission Electron Microscope.

Western blot

Cells were harvested in RIPA buffer (50 mM Tris pH 7.4, 150 mM NaCl (Merck #1064041000), 0,5% sodium deoxycholate (Sigma-Aldrich #30970), 1% NP-40 (Sigma-Aldrich #I3091), 1 mM EDTA (VWR #20302-293), 0,1% SDS (Sigma-Aldrich #L3771) containing 1x protease inhibitor (Merck #11697498001) and 1x phosphatase inhibitor (Merck #4906845001). 20 µg of lysate was loaded on SDS-PAGE gel (BioRad #5671095) and proteins transferred to a PVDF membrane (Merck #IPFL00010) which was blocked using 5x v/v casein blocking buffer in PBS for 1 h at room temperature. The obtained membranes were immunoblotted using primary and secondary antibodies with washing steps using PBST (1x Phosphate-Buffered Saline with 1% Tween20 (Sigma-Aldrich #P1379)). Membranes were analysed using the Odyssey CLx imaging system (Li-cor biosciences) and protein levels were quantified by densitometry with ImageStudio Lite software (Li-cor biosciences).

Macro-mitophagy analysis

siRNA knockdown was conducted as previously described in U2OS-IMLS cells seeded in complete media supplemented with 100 ng/ml doxycycline. Culture media was replaced 24 h after transfection and 1 mM DFP (Sigma-Aldrich #379409) treatment was added after 48 h. For U2OS-IMLS cells expressing PARKIN, 20 µM CCCP (Enzo Life Sciences #BML-CM124-0500) was used for 16 h and 10 µM Q-VD-OPh (Sigma-Aldrich #SML0063-1MG) pan-caspase inhibitor was included to support cell survival[11,37]. Control wells with 100 nM BafA1 (AH diagnostics #BML-CM110-0100) were dosed 2 h prior to fixation. After 72 h, cells were washed with PBS pH 7 and fixed in warm (≈37°C) 3.7% PFA in 0.2 M HEPES (pH 7) for 15 min at 37°C. After washing with PBS, cells were incubated with 2 µg/ml Hoechst and widefield images were obtained using a high-content imaging microscope. The area of red-only puncta per cell (which represent mitochondria delivered to lysosomes as the EGFP signal is quenched in the acidic lysosome) was quantified using a Cell Profiler pipeline. Addition of BafA1 was used as a control to confirm that the mCherry-only puncta corresponded to lysosomal structures.

Halo assay for mitophagy flux

siRNA knockdown was conducted as previously described in U2OS cells expressing the pSu9-Halo-mGFP reporter. 48 h after transfection culture media was changed to contain 100 nM tetramethylrhodamine (TMR)-conjugated Halo ligand (Promega #G8251). After 20 min incubation, cells were washed twice with PBS and the media replaced with either media containing no treatment, 1 mM DFP or 1 mM DMOG. 72 h after transfection cells were harvested and western blot conducted (as described earlier). Membranes were incubated with the Halo Tag antibody and actin antibody. Membranes were imaged using the Chemidoc MP system (Bio-Rad) and band intensity quantified in Image Lab 6.1 (Bio-Rad). Bands were normalised to actin loading control. The percentage cleaved Halo was calculated by the formula (Free Halo / (Free Halo + Full Length)) x 100.

Oxygen consumption rate measurement by Seahorse XF analyser

U2OS cells were seeded in complete medium at the density of $4x10^4$ cells/well into XF24 cell culture microplates (Agilent #100777-004). The sensor cartridge was hydrated for 24 h using XF calibrant in a 37°C non-CO_2 incubator. Before analysis, cell medium was replaced by warm (≈37°C) DMEM without Sodium Bicarbonate (pH 7.4) and placed for 1 h in a 37°C non-CO_2 incubator. Each measurement cycle consisted of a mixing time of 3 min and data acquisition period of 3 min (three data points). OCR results refer to the average rates during each measurement cycle. The final concentration for each mitochondrial inhibitor used in this assay was 1.5 µM Oligomycin A (SelleckChem #S1478), 1 µM CCCP, 0.5 µM Rotenone (Sigma Aldrich #R8875-1G) and 0.5 µM Antimycin (Sigma Aldrich #A8674). Four baseline measurements were performed before adding each compound and three response measurements were taken after each compound was added. Data analysis was performed using Seahorse Analytics software available at *https://seahorseanalytics.agilent.com/* and OCR data was normalised to protein concentration in each well.

Extracellular acidification rate (ECAR) measurement by Seahorse XF analyser

U2OS cells were seeded in complete medium at the density of $4x10^4$ cells/well into XF24 cell culture microplates. The sensor cartridge was hydrated for 24 h using XF calibrant in a 37°C non-CO_2 incubator. Before analysis, cell medium was replaced by warm (≈37°C) XF DMEM media (Seahorse Bioscience #102353-100) supplemented with 2 mM L-Glutamine (BioNordika #BE17-605E) and pH adjusted to 7.4. The final concentration for each reagent used in this assay was 11 mM Glucose, 1.3 µM Oligomycin A, 0.1 M 2-Deoxy-Glucose (2-DG; Sigma Aldrich #D8375-1G)[38]. Each measurement cycle consisted of a mixing time of 3 min and data acquisition period of 3 min (four data points). ECAR results refers to the average rates during each measurement cycle. Five baseline measurements were performed before adding each compound and four response measurements were taken after each compound was added. Data was normalised to protein concentration using Seahorse Analytics software available at *https://seahorseanalytics.agilent.com/* and the glycolysis rate was calculated by subtracting the ECAR value after 2-DG treatment from the ECAR value after addition of glucose.

Purification of crude mitochondrial fraction

To purify crude mitochondrial fraction, cells expressing EGFP (control), mScarlet-RAB27A, SYTL5-EGFP and SYTL5(ΔC2AB)-EGFP were harvested from one 150 mm (80-90% confluency) dish, washed twice with ice cold homogenisation buffer (210 mM mannitol (Sigma Aldrich #M4125), 70 mM sucrose (Sigma Aldrich #S0389), 5 mM HEPES pH 7.12 at 25°C) and harvested in 1 mL homogenisation buffer supplemented (HBS) with 1 mM EGTA (Sigma Aldrich #E3889) and 1x protease inhibitor. The obtained cell lysate was further mechanically homogenised at 4°C using a

cell homogeniser (Isobiotech) equipped with a 16 µm clearance ball by repeatedly passing the cell lysate for 10x repeats with the aid of 2 disposable syringes. The homogenised solution was further spun down at 1500xg for 3 min at 4°C to collect the TCL and the obtained supernatant collected and spun down at 13,000xg for 20 min. The obtained supernatant corresponds to the cytosolic fraction and the pellet was resuspended in 2 mL HBS and spun down at 13,000xg for 20 min. The obtained pellet corresponds to the enriched mitochondrial fraction and was resuspended in 900 µL HBS. 50 µL of each cellular fraction was resuspended in 30 µL 2x SDS-sample buffer and boiled at 100°C for 5 min and further analysed using SDS-PAGE.

GFP-TRAP and FLAG immunoprecipitation

Cells expressing EGFP were harvested from a 100 mm dish (80-90% confluency), washed with ice cold PBS and scraped using ice cold isolation buffer (1% NP-40, 2 mM EDTA, 136 mM NaCl, 20 mM Tris-HCl pH 7.4, 10% glycerol, 1x protease inhibitor and 1x phosphatase inhibitor). Cell lysate was spun down at 20,000xg for 10 min and the supernatant added to 25 µL equilibrated GFP-trap agarose beads (Chromotek #gta-20). Samples were rotated end-over-end for 1 h at 4°C. After 4x washing steps, the beads were collected by centrifugation at 2700xg for 1 min, resuspended in 30 µL 2x SDS-sample buffer and boiled at 100 °C for 5 min. The obtained supernatant was analysed by SDS-PAGE.

U2OS cells expressing pLVX-CMV-SYTL5-EGFP-3xFLAG, pLVX-CMV-SYTL5(ΔC2AB)-EGFP-3xFLAG and pLVX-CMV-SYTL5(ΔSHD)-EGFP-3xFLAG were harvested from a 150 mm dish (80-90% confluency), washed 2x with cold PBS and scraped using 1 ml of cold lysis buffer (50 mM Tris-HCl, pH 7.4,150 mM NaCl, 1% Triton X-100, 5 mM $CaCl_2$ (Merck #1023821000, and 1x protease inhibitor. Cell lysates were spun down at 20,000xg for 10 min and the resulting supernatants added to 40 µL of pre-washed anti-FLAG M2-Agarose Affinity Gel (Sigma Aldrich #FLAGIPT-1). Samples were rotated end-over-end for 2 h at 4°C. After 3x washing steps, the affinity gel was centrifuged at 5000xg for 30 seconds and the FLAG fusion proteins eluted using 3x FLAG peptide according to manufacturer's protocol. The eluted FLAG fusion proteins were diluted in 4 ml 1x TBST supplemented with 3% BSA and 5 mM $CaCl_2$.

I*n-vitro* protein-lipid binding assay

Eluted FLAG fusion proteins (SYTL5-EGFP-3xFLAG, SYTL5(ΔC2AB)-EGFP-3xFLAG and SYTL5(ΔSHD)-EGFP-3xFLAG were diluted in 1x TBST supplemented with 3% BSA and 5 mM $CaCl_2$. PIP strips (Echelon Biosciences #P-6001) and membrane lipid strips (Echelon Biosciences #P-6002) were blocked in 1x TBST supplemented with 3% BSA for 1 h at room temperature and incubated with the diluted FLAG fusion protein for 1 h at 4°C with gentle agitation. Lipid membranes were washed 3x with TBST and incubated with FLAG Tag primary antibody for 1 h at room temperature and detected using SuperSignal West Dura Extended Duration Substrate (Thermo Fisher Scientific #34076).

LC-MS/MS analysis of SYTL5-EGFP interactome

Cells expressing SYTL5-EGFP or EGFP (control) were harvested using NP-40 lysis buffer (10 mM Tris-HCl pH 7.5, 150 mM NaCl, 0.5 mM EDTA, 0.5% NP-40, 1x protease inhibitor. SYTL5-EGFP was immunoprecipitated using GFP-Trap agarose beads according to the manufacturer's protocol. The obtained beads were washed twice with 50 mM ammonium bicarbonate, reduced, alkylated and further digested by trypsin for overnight at 37 °C. Digested peptides were transferred to a new tube, acidified and the peptides were de-salted for MS analysis.

Peptide samples were dissolved in 10 µl 0.1% formic buffer and 3 µl was loaded for MS analysis. LC-MS/MS analysis of the resulting peptides was performed using an Easy nLC1000 liquid chromatography system (Thermo Electron) coupled to a QExactive HF Hybrid Quadrupole-Orbitrap mass spectrometer (Thermo Electron) with a nanoelectrospray ion source (EasySpray,

Thermo Electron). The LC separation of peptides was performed using an EasySpray C18 analytical column (2 µm particle size, 100 Å, 75 µm inner diameter and 25 cm (Thermo Fisher Scientific). Peptides were separated over a 90min gradient from 2% to 30% (v/v) ACN in 0.1% (v/v) FA, after which the column was washed using 90% (v/v) ACN in 0.1% (v/v) FA for 20 min (flow rate 0.3 µL/min). All LC-MS/MS analyses were operated in data-dependent mode where the most intense peptides were automatically selected for fragmentation by high-energy collision-induced dissociation.

Raw files from LC-MS/MS analyses were submitted to MaxQuant 1.6.17.0 software[39] for peptide/protein identification. Parameters were set as follow: Carbamidomethyl (C) was set as a fixed modification and PTY; protein N-acetylation and methionine oxidation as variable modifications. First search error window of 20 ppm and mains search error of 6 ppm. Trypsin without proline restriction enzyme option was used, with two allowed miscleavages. Minimal unique peptides were set to one, and FDR allowed was 0.01 (1%) for peptide and protein identification. The Uniprot human database was used. Generation of reversed sequences was selected to assign FDR rates. Further analysis was performed with Perseus[40], limma/voom[41] and Package R[42]. Volcano plots were plotted with EnhancedVolcano[43]. GO analysis was performed with shinyGO[44].

Bulk gene expression analysis – normal and tumor tissue

Bulk gene expression distribution in healthy/normal tissue samples was collected from GTEx v8 (PMID: 26484571). We utilised a combined RNA-seq expression dataset of TCGA and GTEx samples available through the Xena platform to investigate SYTL5 and RAB27A expression in normal and tumor tissue (PMID: 32444850). Here, data from a total of n = 77 samples provided normal adrenal gland expression (GTEx), and a total of n = 128 samples provided expression in adrenocortical carcinoma samples (TCGA-ACC). Survival data from samples in the TCGA-ACC cohort (one record per patient) was obtained using the TCGABiolinks R package[45]. Survival curve analysis was performed using GraphPad Prism 8.0.1 using Logrank test (Mantel-Cox).

Cortisol assay

To measure cortisol in cell culture supernates, siRNA knockdown by reverse transfection with siSYTL5 and siRAB27A was conducted as described earlier in NCI-H295R cells. Cells were harvested with TNTE Lysis Buffer. Cortisol from lysates was measured using the R&D Systems® Cortisol Immunoassay kit (# KGE008B) as described in the protocol provided from the company. Controls were performed using cells treated with 50 uM Forskolin as a positive control to stimulate cortisol secretion[46], or 10 uM mitotane to inhibit cortisol production[47].

Statistical analysis

Statistical analysis was performed with GraphPad Prism (8.0.1, 9.3.1 and 10.2.0 versions) and the tests used are indicated in the respective figure legends. All values come from distinct samples.

**** = p<0.0001, *** = p<0.001, ** = p<0.01, * = p< 0.05.

Supplementary figures

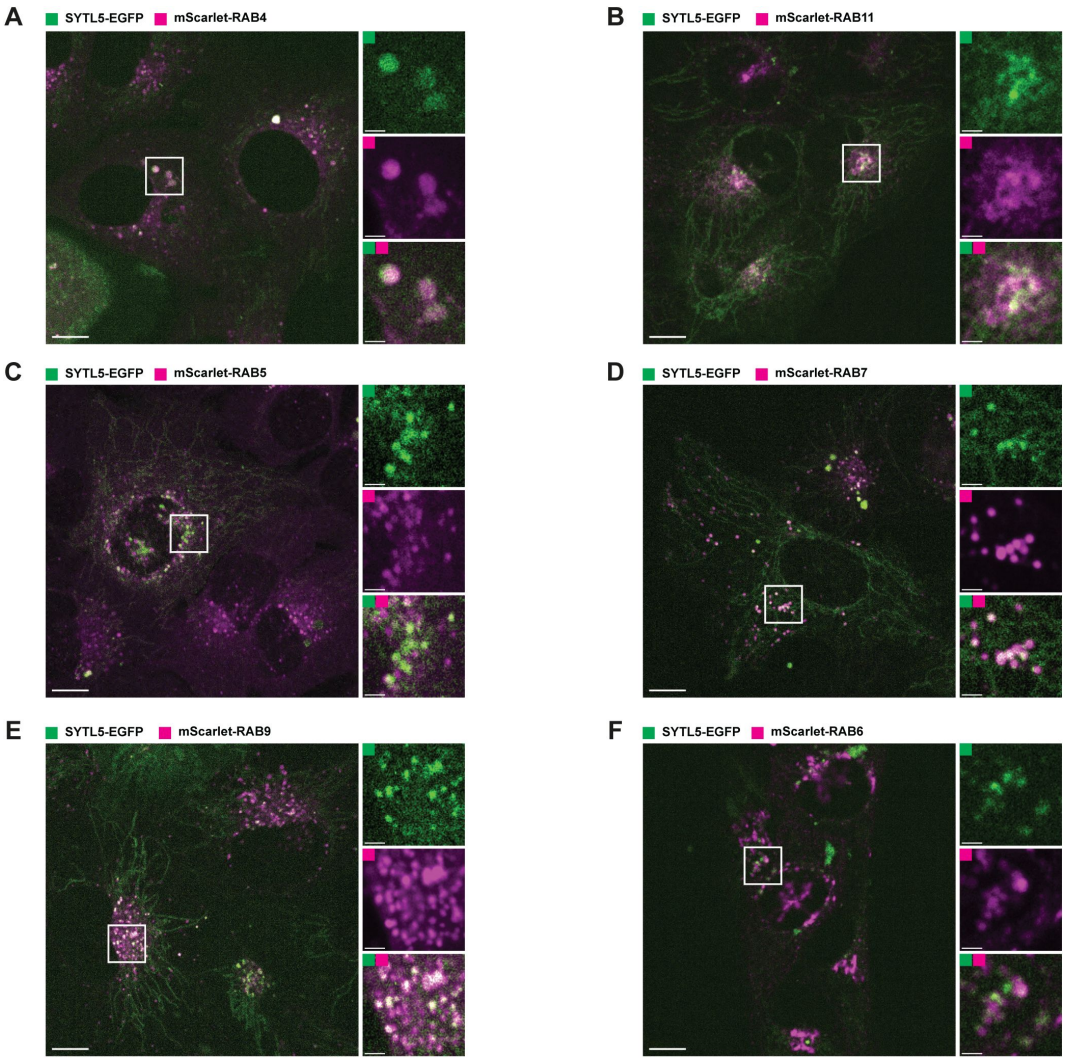

Figure S1.

A-F. SYTL5-EGFP expression was induced for 24 h with 100 ng/ml doxycycline in U2OS cells with stable inducible expression of SYTL5-EGFP and constitutive expression of mScarlet-RAB4 (A), mScarlet-RAB11 (B), mScarlet-RAB5 (C), mScarlet-RAB7 (D), mScarlet-RAB9 (E) or mScarlet-RAB6 (F) followed by live confocal microscopy imaging analysis. Scale bars: 10 µm, 2 µm (insets).

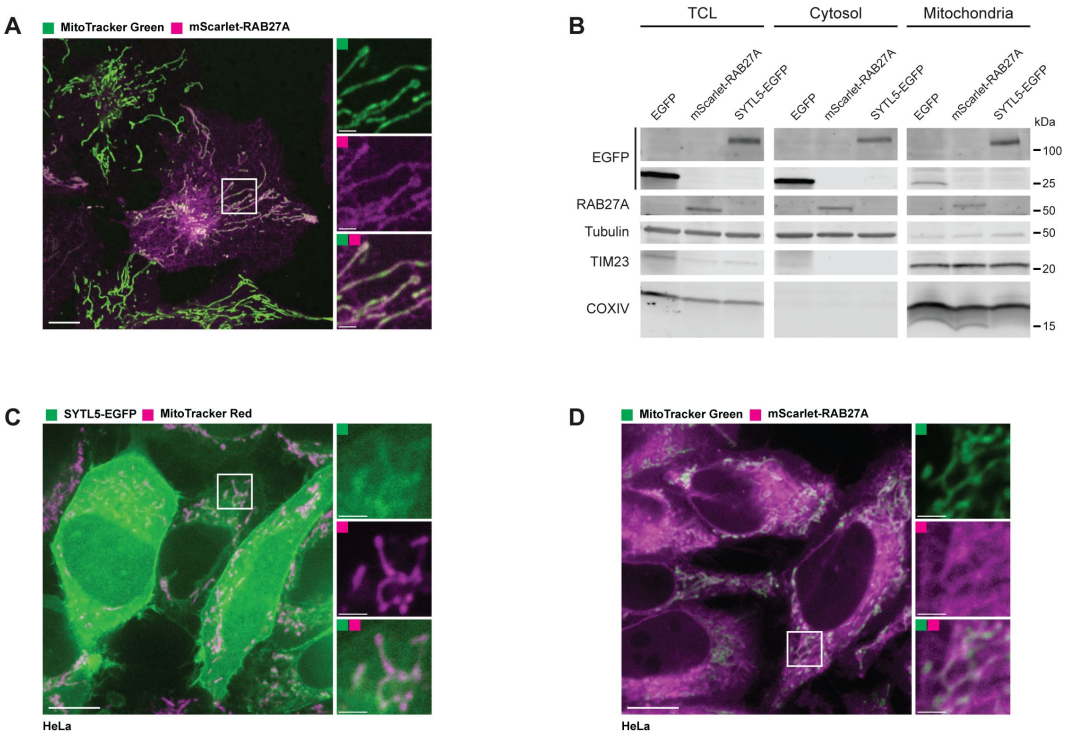

Figure S2.

A. Live confocal microscopy imaging of U2OS constitutively expressing mScarlet-RAB27A co-stained with MitoTracker green added 30 min before imaging. Scale bars: 10 μm, 2 μm (insets). B. Total cell lysate (TCL), cytosol, and a crude mitochondria fraction from U2OS control cells and cells with stable expression of mScarlet-RAB27A or SYTL5-EGFP were analysed by western blotting for EGFP, RAB27A, tubulin, TIM23 and COXIV. C. Live confocal microscopy imaging of HeLa constitutively expressing SYTL5-EGFP co-stained with MitoTracker Red added 30 min before imaging. Scale bars: 10 μm, 2 μm (insets). D. Live confocal microscopy imaging of HeLa constitutively expressing mScarlet-RAB27A co-stained with MitoTracker green added 30 min before imaging. Scale bars: 10 μm, 2 μm (insets).

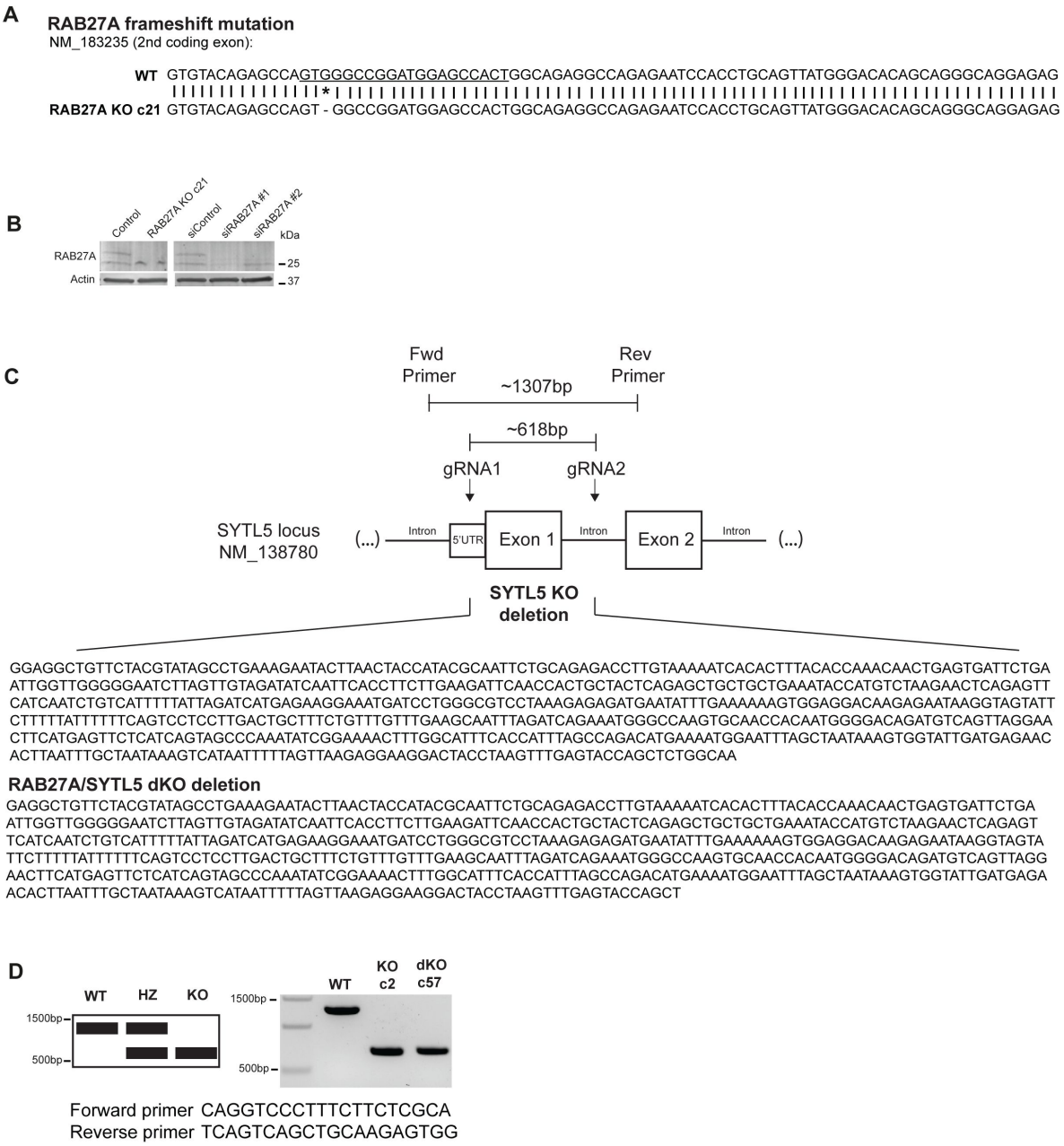

Figure S3.

A. RAB27A KO validation by genotyping. The WT RAB27A gDNA sequence was aligned with the RAB27A KO clone 21(c21) gDNA sequence. CRISPR/Cas9 editing produced an indel (single nucleotide deletion indicated by *) in a genomic location shared between all RAB27A isoforms. gRNA targeting region is underlined in the WT RAB27A gDNA sequence. B. RAB27A KO validation by western blot. Cell lysates from U2OS control cells and RAB27A KO cells (c21) were compared to cell lysates where RAB27A was depleted for 72 h using 2 independent siRNAs and probed with RAB27 and actin antibodies. C. SYTL5 CRISPR/Cas9 exon deletion was performed using two gRNA simultaneously. These gRNA target the 5'UTR or intronic regions of SYTL5 (transcript NM_138780) that are shared by all SYTL5 isoforms. Genomic deletion validation and individual clone genotyping was performed using a primer pair that flanked the region to be edited (about 1307 bp length between these primer binding sites). D. SYTL5 KO validation was performed with conventional PCR reaction. A PCR product of 1307 bp is expected for wild-type U2OS gDNA, while a PCR product of about 618 bp is expected if a clone has a deletion in the targeted region. This method was used to validate the SYTL5 KO clone2 and for dKO RAB27A/SYTL5 clone57. The deleted sequence includes a coding exon from SYTL5, resulting in a non-functional SYTL5 protein.

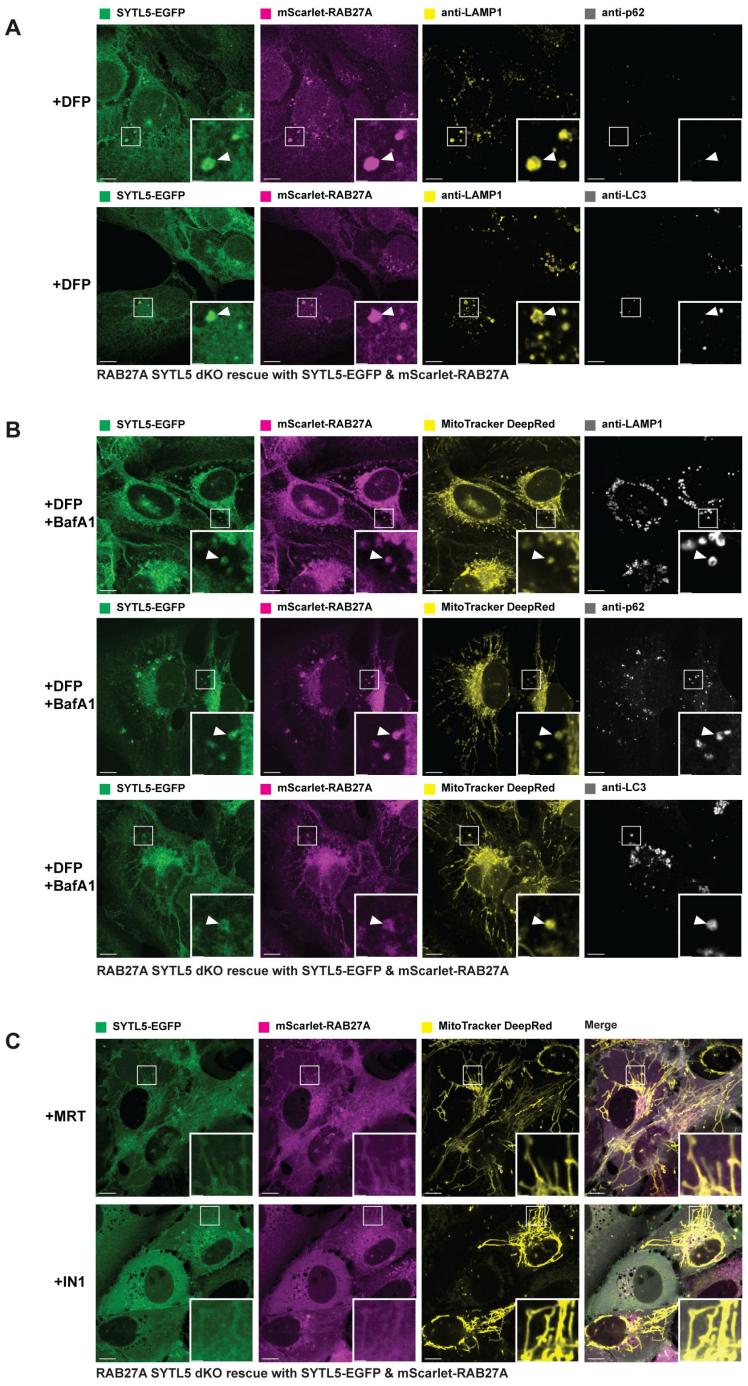

Figure S4.

A. SYTL5/RAB27A dKO U2OS cells rescued with SYTL5-EGFP and mScarlet-RAB27A were treated with 1 mM DFP for 24 h. Fixed cells were stained with a LAMP1 antibody in addition to either p62 (upper panel) or LC3 (lower panels) antibodies and imaged by confocal microscopy. Arrowheads point to SYTL5/RAB27A-positive structures. Scale bars: 10 µm, 2 µm (insets). B. SYTL5/RAB27A dKO U2OS cells rescued with SYTL5-EGFP and mScarlet-RAB27A were treated with 1 mM DFP for 24 h and 100 nM BafA1 for the final 4 h. All cells were stained with 50 nM MitoTracker DR 30 min prior to fixing. Fixed cells were stained with either LAMP1 (upper panel), p62 (middle panel) or LC3 (lower panel) antibody and imaged by confocal microscopy. Arrowheads point to SYTL5/RAB27A-positive structures. Scale bars: 10 µm, 2 µm (insets). C. SYTL5/RAB27A dKO U2OS cells rescued with SYTL5-EGFP and mScarlet-RAB27A were treated with 1 µM MRT68921 for 2 h (upper panel) or 5 µM Vps34-IN1 for 2 h (lower panel). All cells were stained with 50 nM MitoTracker DR 30 min prior to live imaging confocal microscopy. Scale bars: 10 µm, 2 µm (insets).

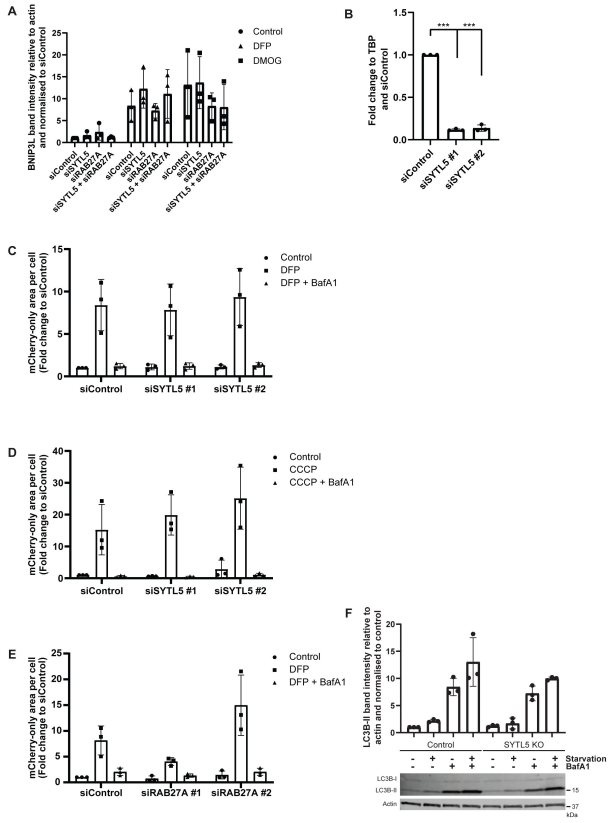

Figure S5.

B. U2OS cells were transfected with 20 nM control siRNA, SYTL5 siRNA #1 or RAB27A siRNA #1 for 48 h followed by 24 h incubation with 1 mM DFP or 1 mM DMOG. Cell lysates were analysed by western blot for BNIP3L. Actin was used as a loading control. Error bars represent the mean with standard deviation between replicates (n=3). C. U2OS cells were transfected with 20 nM control siRNA or SYTL5 siRNA oligos for 72 h. Transfection efficiency was analysed by qPCR where the relative mRNA expression of SYTL5 was normalised to the expression levels of TBP and siControl. Error bars represent the standard deviation between replicates (n=3). Significance was determined by one-way ANOVA followed by Dunnett multiple comparison test, *** = p<0.001. D. U2OS cells expressing the mitochondrial matrix reporter NIPSNAP1[1–53]-EGFP-mCherry[29] (referred to as IMLS cells) were transfected with 20 nM control siRNA or SYTL5 siRNA oligos for 48 h before 24 h incubation with 1 mM DFP in the absence or presence of 100 nM BafA1 for the last 2 h. After fixation, cell nuclei were stained with Hoechst and widefield images were obtained using a high-content imaging microscope. The area of red-only puncta per cell (>1000 cells analysed, represent mitochondria delivered to lysosomes as the EGFP signal is quenched in the acidic lysosome) was quantified using a Cell Profiler pipeline. The obtained results were normalised to the control siRNA and error bars represent the mean with standard deviation between replicates (n=3). Significance was determined by two-way ANOVA followed by Bonferroni multiple comparison test. E. U2OS IMLS cells expressing PARKIN were transfected with 20 nM control siRNA or SYTL5 siRNA oligos for 48 h before a 16 h incubation with 20 μM CCCP to induce mitophagy, with treatment with 100 nM BafA1 or not for the last 2 h. The area of red-only puncta per cell (>1000 cells analysed) was quantified using Cell Profiler from widefield images obtained using a high-content imaging microscope. The obtained results were normalised to the control siRNA and error bars represent the mean with standard deviation between replicates (n=3). Significance was determined by two-way ANOVA followed by Tukey's multiple comparison test. F. U2OS IMLS cells were transfected with 20 nM control siRNA or RAB27A siRNA oligos for 48 h before 24 h incubation with 1 mM DFP in the absence or presence of 100 nM BafA1 for the last 2 h. After fixation, cell nuclei were stained with Hoechst and widefield images were obtained using a high-content imaging microscope. The area of red-only puncta per cell (>1000 cells analysed) was quantified using a Cell Profiler pipeline. The obtained results were normalised to the siControl, and error bars represent the mean with standard deviation between replicates (n=3). Significance was determined by two-way ANOVA followed by Bonferroni multiple comparison test. G. WT (control) or SYTL5 KO U2OS cells were starved in EBSS for 4 h or incubated with complete medium in the presence or absence of 100 nM BafA1 the last 2 h. Cell lysates were harvested and analysed by western blot for LC3B and actin proteins. LC3B-II band intensity was quantified relative to actin and normalised to control. Error bars represent the mean with standard deviation between replicates (n=3). Significance was determined by one-way ANOVA followed by Bonferroni multiple comparison test.

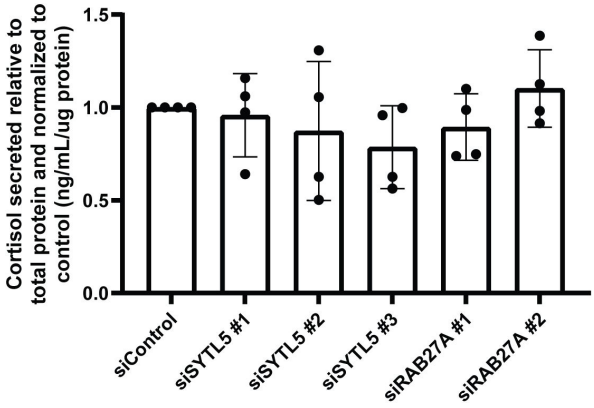

Figure S6

NCl-H295R cells were transfected with 20 nM control siRNA, SYTL5 siRNA or RAB27A siRNA oligos for 72 h.

Cortisol secretion was measured and normalised to siControl. Error bars represent the mean with standard deviation between replicates (n=4).

Acknowledgements

We thank Jenni Lane for assisting with EM sample preparation, Sachin Singh and Tuula Nyman at the OUS Proteomics Core Facility for assisting with mass spectrometry-based proteomic experiments, Ankush Sharma for help with analysis of mass spectrometry data, Anna Lång at ALM Core Facility Gaustad for assisting with widefield microscopy experiments, Santosh Phuyal for experimental assistance and Serhiy Pankiv for providing the lentiviral mScarlet-RAB expression constructs. We also thank Patricia González-Rodríguez for providing us with the U2OS pSu9-HaloTag7-mGFP cells and Viola Nähse for her contributions and advice regarding CRISPR knock-in strategies.

This project was funded by the Research Council of Norway through its Centres of Excellence funding scheme (project number 262652) and FRIPRO grant (project number 249753), the Norwegian Cancer Society (project number 190251), Marie Skłodowska-Curie ETN grant under the European Union's Horizon 2020 Research and Innovation Programme (Grant Agreement No 765912 DRIVE) and by the University of Oslo Scientia Fellow program through the MSC scheme – Co-funding of Regional, National and International Programmes (COFUND). Mass spectrometry-based proteomic analyses were performed by the Proteomics Core Facility, Department of Immunology, University of Oslo/Oslo University Hospital, which is supported by the Core Facilities program of the South-Eastern Norway Regional Health Authority. This core facility is also a member of the National Network of Advanced Proteomics Infrastructure (NAPI), which is funded by the Research Council of Norway INFRASTRUKTUR-program (project number: 295910).

Additional information

Author contributions

A.L., L.S.J., L.T.M. and A.S. designed and conceived the experimental work. A.L., L.S.J., L.T.M.,

M.Y.W.N. and S.J.R. performed the experiments and data analyses. S.S. carried out MS and GO term enrichment data analysis. S.N. provided GTEx and TCGA data analysis. E.L.E. performed and analysed CLEM data. A.L., L.S.J. and A.S. wrote the manuscript.

Funding

The Research Council of Norway (262652)

The Research Council of Norway (249753)

Norwegian Cancer Society (190251)

Southern and Eastern Norway Regional Health Authority (2020032)

Additional files

Supplementary video 1. *Live confocal microscopy imaging tracking SYTL5 vesicle movement along filaments positive for MitoTracker red.*

References

1 Kuroda T. S., Fukuda M., Ariga H., Mikoshiba K (2002) **Synaptotagmin-like protein 5: a novel Rab27A effector with C-terminal tandem C2 domains** *Biochem Biophys Res Commun* **293**:899–906 https://doi.org/10.1016/s0006-291x(02)00320-0 | Google Scholar

2 Kuroda T. S., Fukuda M., Ariga H., Mikoshiba K (2002) **The Slp homology domain of synaptotagmin-like proteins 1-4 and Slac2 functions as a novel Rab27A binding domain** *J. Biol. Chem* **277**:9212–9218 https://doi.org/10.1074/jbc.M112414200 | Google Scholar

3 Nalefski E. A., Falke J. J (1996) **The C2 domain calcium-binding motif: structural and functional diversity** *Protein Sci* **5**:2375–2390 https://doi.org/10.1002/pro.5560051201 | Google Scholar

4 Gálvez-Santisteban M., et al. (2012) **Synaptotagmin-like proteins control the formation of a single apical membrane domain in epithelial cells** *Nat. Cell Biol* **14**:838–849 https://doi.org/10.1038/ncb2541 | Google Scholar

5 Fukuda M (2002) **The C2A domain of synaptotagmin-like protein 3 (Slp3) is an atypical calcium-dependent phospholipid-binding machine: comparison with the C2A domain of synaptotagmin I** *Biochem. J* **366**:681–687 https://doi.org/10.1042/bj20020484 | Google Scholar

6 Yu M., et al. (2007) **Exophilin4/Slp2-a targets glucagon granules to the plasma membrane through unique Ca2+-inhibitory phospholipid-binding activity of the C2A domain** *Molecular biology of the cell* **18**:688–696 https://doi.org/10.1091/mbc.e06-10-0914 | Google Scholar

7 Fukuda M (2013) **Rab27 effectors, pleiotropic regulators in secretory pathways** *Traffic* **14**:949–963 https://doi.org/10.1111/tra.12083 | Google Scholar

8 Montava-Garriga L., Ganley I. G (2020) **Outstanding Questions in Mitophagy: What We Do and Do Not Know** *J. Mol. Biol* **432**:206–230 https://doi.org/10.1016/j.jmb.2019.06.032 | Google Scholar

9 Martínez-Reyes I., Chandel N. S (2020) **Mitochondrial TCA cycle metabolites control physiology and disease** *Nat Commun* **11** https://doi.org/10.1038/s41467-019-13668-3 | Google Scholar

10 Allen G. F., Toth R., James J., Ganley I. G (2013) **Loss of iron triggers PINK1/Parkin-independent mitophagy** *EMBO Rep* **14**:1127–1135 https://doi.org/10.1038/embor.2013.168 | Google Scholar

11 Lazarou M., et al. (2015) **The ubiquitin kinase PINK1 recruits autophagy receptors to induce mitophagy** *Nature* **524**:309–314 https://doi.org/10.1038/nature14893 | Google Scholar

12 Le Guerroué F., et al. (2017) **Autophagosomal Content Profiling Reveals an LC3C-Dependent Piecemeal Mitophagy Pathway** *Mol. Cell* **68**:786–796 https://doi.org/10.1016/j.molcel.2017.10.029 | Google Scholar

13 Abudu Y. P., et al. (2021) **SAMM50 acts with p62 in piecemeal basal- and OXPHOS-induced mitophagy of SAM and MICOS components** *J. Cell Biol* **220** https://doi.org/10.1083/jcb.202009092 | Google Scholar

14 Neuspiel M., et al. (2008) **Cargo-selected transport from the mitochondria to peroxisomes is mediated by vesicular carriers** *Curr. Biol* **18**:102–108 https://doi.org/10.1016/j.cub.2007.12.038 | Google Scholar

15 Soubannier V., et al. (2012) **A vesicular transport pathway shuttles cargo from mitochondria to lysosomes** *Curr. Biol* **22**:135–141 https://doi.org/10.1016/j.cub.2011.11.057 | Google Scholar

16 Prashar A., et al. (2024) **Lysosomes drive the piecemeal removal of mitochondrial inner membrane** *Nature* **632**:1110–1117 https://doi.org/10.1038/s41586-024-07835-w | Google Scholar

17 Choong C. J., et al. (2021) **Alternative mitochondrial quality control mediated by extracellular release** *Autophagy* **17**:2962–2974 https://doi.org/10.1080/15548627.2020.1848130 | Google Scholar

18 Phinney D. G., et al. (2015) **Mesenchymal stem cells use extracellular vesicles to outsource mitophagy and shuttle microRNAs** *Nat Commun* **6** https://doi.org/10.1038/ncomms9472 | Google Scholar

19 Jiao H., et al. (2021) **Mitocytosis, a migrasome-mediated mitochondrial quality-control process** *Cell* **184**:2896–2910 https://doi.org/10.1016/j.cell.2021.04.027 | Google Scholar

20 Youle R. J., Narendra D. P. (2011) **Mechanisms of mitophagy** *Nat. Rev. Mol. Cell Biol* **12**:9–14 https://doi.org/10.1038/nrm3028 | Google Scholar

21 Ding W. X., Yin X. M (2012) **Mitophagy: mechanisms, pathophysiological roles, and analysis** *Biol. Chem* **393**:547–564 https://doi.org/10.1515/hsz-2012-0119 | Google Scholar

22 Liberti M. V., Locasale J. W (2016) **The Warburg Effect: How Does it Benefit Cancer Cells?** *Trends Biochem. Sci* **41**:211–218 https://doi.org/10.1016/j.tibs.2015.12.001 | Google Scholar

23 Else T., et al. (2014) **Adrenocortical carcinoma** *Endocr. Rev* **35**:282–326 https://doi.org/10.1210/er.2013-1029 | Google Scholar

24 Miller W. L (2013) **Steroid hormone synthesis in mitochondria** *Mol Cell Endocrinol* **379**:62–73 https://doi.org/10.1016/j.mce.2013.04.014 | Google Scholar

25 Munson M. J., et al. (2021) **GAK and PRKCD are positive regulators of PRKN-independent mitophagy** *Nat Commun* **12** https://doi.org/10.1038/s41467-021-26331-7 | Google Scholar

26 Wandinger-Ness A., Zerial M (2014) **Rab proteins and the compartmentalization of the endosomal system** *Cold Spring Harb. Perspect. Biol* **6** https://doi.org/10.1101/cshperspect.a022616 | Google Scholar

27 Baietti M. F., et al. (2012) **Syndecan–syntenin–ALIX regulates the biogenesis of exosomes** *Nat. Cell Biol* **14**:677–685 https://doi.org/10.1038/ncb2502 | Google Scholar

28 Yim W. W.-Y., Yamamoto H., Mizushima N (2022) **A pulse-chasable reporter processing assay for mammalian autophagic flux with HaloTag** *eLife* **11**:e78923 https://doi.org/10.7554/eLife

.78923 | Google Scholar

29 Abudu Princely, et al. (2019) **NIPSNAP1 and NIPSNAP2 Act as "Eat Me" Signals for Mitophagy** *Dev. Cell* **49**:509–525 https://doi.org/10.1016/j.devcel.2019.03.013 | Google Scholar

30 Hill B. G., et al. (2012) **Integration of cellular bioenergetics with mitochondrial quality control and autophagy** *Biol. Chem* **393**:1485–1512 https://doi.org/10.1515/hsz-2012-0198 | Google Scholar

31 Tang Z., et al. (2017) **GEPIA: a web server for cancer and normal gene expression profiling and interactive analyses** *Nucleic Acids Res* **45**:W98–w102 https://doi.org/10.1093/nar/gkx247 | Google Scholar

32 Wang T., Rainey W. E (2012) **Human adrenocortical carcinoma cell lines** *Mol Cell Endocrinol* **351**:58–65 https://doi.org/10.1016/j.mce.2011.08.041 | Google Scholar

33 Ishida M., Arai S. P., Ohbayashi N., Fukuda M (2014) **The GTPase-deficient Rab27A(Q78L) mutant inhibits melanosome transport in melanocytes through trapping of Rab27A effector protein Slac2-a/melanophilin in their cytosol: development of a novel melanosome-targetinG tag** *J. Biol. Chem* **289**:11059–11067 https://doi.org/10.1074/jbc.M114.552281 | Google Scholar

34 Yamano K., et al. (2018) **Endosomal Rab cycles regulate Parkin-mediated mitophagy** *eLife* **7** https://doi.org/10.7554/eLife.31326 | Google Scholar

35 Key J., et al. (2019) **Ubiquitylome profiling of Parkin-null brain reveals dysregulation of calcium homeostasis factors ATP1A2, Hippocalcin and GNA11, reflected by altered firing of noradrenergic neurons** *Neurobiol. Dis* **127**:114–130 https://doi.org/10.1016/j.nbd.2019.02.008 | Google Scholar

36 Yim W. W., Yamamoto H., Mizushima N (2022) **A pulse-chasable reporter processing assay for mammalian autophagic flux with HaloTag** *eLife* **11** https://doi.org/10.7554/eLife.78923 | Google Scholar

37 Caserta T. M., Smith A. N., Gultice A. D., Reedy M. A., Brown T. L (2003) **Q-VD-OPh, a broad spectrum caspase inhibitor with potent antiapoptotic properties** *Apoptosis* **8**:345–352 https://doi.org/10.1023/a:1024116916932 | Google Scholar

38 TeSlaa T., Teitell M. A (2014) **Techniques to monitor glycolysis** *Methods Enzymol* **542**:91–114 https://doi.org/10.1016/b978-0-12-416618-9.00005-4 | Google Scholar

39 Cox J., Mann M (2008) **MaxQuant enables high peptide identification rates, individualized p.p.b.-range mass accuracies and proteome-wide protein quantification** *Nat. Biotechnol* **26**:1367–1372 https://doi.org/10.1038/nbt.1511 | Google Scholar

40 Tyanova S., et al. (2016) **The Perseus computational platform for comprehensive analysis of (prote)omics data** *Nat. Methods* **13**:731–740 https://doi.org/10.1038/nmeth.3901 | Google Scholar

41 Ritchie M. E., et al. (2015) **limma powers differential expression analyses for RNA-sequencing and microarray studies** *Nucleic Acids Res* **43**:e47 https://doi.org/10.1093/nar/gkv007 | Google Scholar

42 Dessau R. B., Pipper C. B (2008) **[''R"--project for statistical computing]** *Ugeskr. Laeger* **170**:328–330 Google Scholar

43 Blighe Kevin, Myles Lewis S. R. (2021) **EnhancedVolcano: publication-ready volcano plots with enhanced colouring and labeling** *GitHub* https://github.com/kevinblighe/EnhancedVolcano

44 Ge S. X., Jung D., Yao R (2020) **ShinyGO: a graphical gene-set enrichment tool for animals and plants** *Bioinformatics* **36**:2628–2629 https://doi.org/10.1093/bioinformatics/btz931 | Google Scholar

45 Colaprico A., et al. (2016) **TCGAbiolinks: an R/Bioconductor package for integrative analysis of TCGA data** *Nucleic Acids Res* **44**:e71 https://doi.org/10.1093/nar/gkv1507 | Google Scholar

46 Maglich J. M., Kuhn M., Chapin R. E., Pletcher M. T (2014) **More than just hormones: H295R cells as predictors of reproductive toxicity** *Reprod Toxicol* **45**:77–86 https://doi.org/10.1016/j.reprotox.2013.12.009 | Google Scholar

47 Lin C. W., Chang Y. H., Pu H. F (2012) **Mitotane exhibits dual effects on steroidogenic enzymes gene transcription under basal and cAMP-stimulating microenvironments in NCI-H295 cells** *Toxicology* **298**:14–23 https://doi.org/10.1016/j.tox.2012.04.007 | Google Scholar

Author information

Ana Lapao*
Department of Molecular Medicine, Institute of Basic Medical Sciences, Faculty of Medicine, University of Oslo, Oslo, Norway, Centre for Cancer Cell Reprogramming, Institute of Clinical Medicine, Faculty of Medicine, University of Oslo, Oslo, Norway

*The authors contributed equally

Lauren Sophie Johnson*
Department of Molecular Medicine, Institute of Basic Medical Sciences, Faculty of Medicine, University of Oslo, Oslo, Norway, Centre for Cancer Cell Reprogramming, Institute of Clinical Medicine, Faculty of Medicine, University of Oslo, Oslo, Norway, Department of Molecular Cell Biology, Institute for Cancer Research, Oslo University Hospital Montebello, Oslo, Norway

*The authors contributed equally

Laura Trachsel-Moncho
Department of Molecular Medicine, Institute of Basic Medical Sciences, Faculty of Medicine, University of Oslo, Oslo, Norway, Centre for Cancer Cell Reprogramming, Institute of Clinical Medicine, Faculty of Medicine, University of Oslo, Oslo, Norway, Department of Molecular Cell Biology, Institute for Cancer Research, Oslo University Hospital Montebello, Oslo, Norway

Samuel J Rodgers
Centre for Cancer Cell Reprogramming, Institute of Clinical Medicine, Faculty of Medicine, University of Oslo, Oslo, Norway, Department of Molecular Cell Biology, Institute for Cancer Research, Oslo University Hospital Montebello, Oslo, Norway
ORCID iD: 0000-0002-7186-8355

Sakshi Singh
Department of Molecular Medicine, Institute of Basic Medical Sciences, Faculty of Medicine, University of Oslo, Oslo, Norway, Centre for Cancer Cell Reprogramming, Institute of Clinical Medicine, Faculty of Medicine, University of Oslo, Oslo, Norway

Matthew Yoke Wui Ng
Department of Molecular Medicine, Institute of Basic Medical Sciences, Faculty of Medicine, University of Oslo, Oslo, Norway, Centre for Cancer Cell Reprogramming, Institute of Clinical Medicine, Faculty of Medicine, University of Oslo, Oslo, Norway

Sigve Nakken
Centre for Cancer Cell Reprogramming, Institute of Clinical Medicine, Faculty of Medicine, University of Oslo, Oslo, Norway, Department of Tumour Biology, Institute for Cancer Research, Oslo University Hospital, Oslo, Norway, Department of Informatics, University of Oslo, Oslo, Norway
ORCID iD: 0000-0001-8468-2050

Eeva-Liisa Eskelinen
Institute of Biomedicine, University of Turku, Turku, Finland

Anne Simonsen
Department of Molecular Medicine, Institute of Basic Medical Sciences, Faculty of Medicine, University of Oslo, Oslo, Norway, Centre for Cancer Cell Reprogramming, Institute of Clinical Medicine, Faculty of Medicine, University of Oslo, Oslo, Norway, Department of Molecular Cell Biology, Institute for Cancer Research, Oslo University Hospital Montebello, Oslo, Norway
ORCID iD: 0000-0003-4711-7057

For correspondence: anne.simonsen@medisin.uio.no

Editors

Reviewing Editor
Li Yu
Tsinghua University, Beijing, China

Senior Editor
David Ron
University of Cambridge, Cambridge, United Kingdom

Reviewer #1 (Public review):

Summary:

In this study, Ana Lapao et al. investigated the roles of Rab27 effector SYTL5 in cellular membrane trafficking pathways. The authors found that SYTL5 localizes to mitochondria in a Rab27A-dependent manner. They demonstrated that SYTL5-Rab27A positive vesicles

containing mitochondrial material are formed under hypoxic conditions, thus they speculate that SYTL5 and Rab27A play roles in mitophagy. They also found that both SYTL5 and Rab27A are important for normal mitochondrial respiration. Cells lacking SYTL5 undergo a shift from mitochondrial oxygen consumption to glycolysis which is a common process known as the Warburg effect in cancer cells. Based on cancer patient database, the author noticed that low SYTL5 expression is related to reduced survival for adrenocortical carcinoma patients, indicating SYTL5 could be a negative regulator of the Warburg effect and potentially tumorigenesis.

Strengths:

The authors take advantages of multiple techniques and novel methods to perform the experiments.

(1) Live-cell imaging revealed that stably inducible expression of SYTL5 co-localized with filamentous structures positive for mitochondria. This result was further confirmed by using correlative light and EM (CLEM) analysis and western blotting from purified mitochondrial fraction.

(2) In order to investigate whether SYTL5 and RAB27A are required for mitophagy in hypoxic conditions, two established mitophagy reporter U2OS cell lines were used to analyze the autophagic flux.

Weaknesses:

This study revealed a potential function of SYTL5 in mitophagy and mitochondrial metabolism. However, the mechanistic evidence that establishes the relationship between SYTL5/Rab27A and mitophagy is insufficient. The involvement of SYTL5 in ACC needs more investigation. Furthermore, images and results supporting the major conclusions need to be improved.

Comments on revisions: The authors did not revise the paper as suggested.

https://doi.org/10.7554/eLife.105541.2.sa3

Reviewer #2 (Public review):

Summary:

The authors provide convincing evidence that Rab27 and STYL5 work together to regulate mitochondrial activity and homeostasis.

Strengths:

The development of models which allow the function to be dissected, and the rigous approach and testing of mitochondrial activity.

This work is carefully done, and supports the importance of the roles of Rab27A and STYL5.

https://doi.org/10.7554/eLife.105541.2.sa2

Reviewer #3 (Public review):

In the manuscript by Lapao et al., the authors uncover a role for the RAB27A effector protein SYTL5 in regulating mitochondrial function and apparent selective turnover of mitochondrial components. The authors find that SYTL5 localizes to mitochondria in a RAB27A dependent

way and that loss of SYTL5 (or RAB27A) impairs lysosomal turnover of MTCO1 (but not a matrix-based reporter/other mitochondrial proteins). The authors go on to show that loss of SYTL5 impacts mitochondrial respiration and ECAR and as such may influence the Warburg effect and tumorigenesis. Of relevance here, the authors go on to show that SYTL5 expression is reduced in adrenocortical carcinomas and this correlates with reduced survival rates.

As previously reviewed, this is a very intriguing body of work and reveals a new role for SYTL5/RAB27A at the mitochondria. Unfortunately, it appears that SYTL5 is challenging protein to detect endogenously and the authors' cell lines "comprise a heterogenous pool with high variability", which means that a lot of my original concerns remain. It is still also not clear if the conventional autophagy machinery is required for this pathway, especially if SYTL5/RAB27A mitochondrial recruitment is upstream of this. Hopefully, in future work, the authors (and/or others) will be able to address this and build on the mechanisms of this interesting and potentially important pathway.

https://doi.org/10.7554/eLife.105541.2.sa1

Author response:

The following is the authors' response to the original reviews.

> ***Reviewer #1 (Public review):***
>
> *Summary:*
>
> *In this study, Ana Lapao et al. investigated the roles of Rab27 effector SYTL5 in cellular membrane trafficking pathways. The authors found that SYTL5 localizes to mitochondria in a Rab27A-dependent manner. They demonstrated that SYTL5-Rab27A positive vesicles containing mitochondrial material are formed under hypoxic conditions, thus they speculate that SYTL5 and Rab27A play roles in mitophagy. They also found that both SYTL5 and Rab27A are important for normal mitochondrial respiration. Cells lacking SYTL5 undergo a shift from mitochondrial oxygen consumption to glycolysis which is a common process known as the Warburg effect in cancer cells. Based on the cancer patient database, the author noticed that low SYTL5 expression is related to reduced survival for adrenocortical carcinoma patients, indicating SYTL5 could be a negative regulator of the Warburg effect and potentially tumorigenesis.*
>
> *Strengths:*
>
> *The authors take advantage of multiple techniques and novel methods to perform the experiments.*
>
> *(1) Live-cell imaging revealed that stably inducible expression of SYTL5 co-localized with filamentous structures positive for mitochondria. This result was further confirmed by using correlative light and EM (CLEM) analysis and western blotting from purified mitochondrial fraction.*
>
> *(2) In order to investigate whether SYTL5 and Rab27A are required for mitophagy in hypoxic conditions, two established mitophagy reporter U2OS cell lines were used to analyze the autophagic flux.*
>
> *Weaknesses:*
>
> *This study revealed a potential function of SYTL5 in mitophagy and mitochondrial metabolism. However, the mechanistic evidence that establishes the relationship between SYTL5/Rab27A and mitophagy is insufficient. The involvement of SYTL5 in ACC needs*

> *more investigation. Furthermore, images and results supporting the major conclusions need to be improved.*

We thank the reviewer for their constructive comments. We agree that a complete understanding of the mechanism by which SYTL5 and Rab27A are recruited to the mitochondria and subsequently involved in mitophagy requires further investigation. Here, we have shown that SYTL5 recruitment to the mitochondria requires both its lipid-binding C2 domains and the Rab27A-binding SHD domain (Figure 1G-H). This implies a coincidence detection mechanism for mitochondrial localisation of SYTL5. Additionally, we find that mitochondrial recruitment of SYTL5 is dependent on the GTPase activity and mitochondrial localisation of Rab27A (Figure 2D-E). We also identified proteins linked to the cellular response to oxidative stress, reactive oxygen species metabolic process, regulation of mitochondrion organisation and protein insertion into mitochondrial membrane to be enriched in the SYTL5 interactome (Figure 3A and C).

However, less details regarding the mitochondrial localisation of Rab27A are understood. To investigate this, we have now performed a mass spectrometry analysis to identify the interactome of Rab27A (see Author response table 1 below,). U2OS cells with stable expression of mScarlet-Rab27A or mScarlet only, were subjected to immunoprecipitation, followed by MS analysis. Of the 32 significant Rab27A-interacting hits (compared to control), two of the hits are located in the inner mitochondrial membrane (IMM); ATP synthase F(1) complex subunit alpha (P25705), and mitochondrial very long-chain specific acyl-CoA dehydrogenase (VLCAD)(P49748). However, as these IMM proteins are not likely involved in mitochondrial recruitment of Rab27A, observed under basal conditions, we choose not to include these data in the manuscript.

It is known that other RAB proteins are recruited to the mitochondria. During parkin-mediated mitophagy, RABGEF1 (a guanine nucleotide exchange factor) is recruited through its ubiquitin-binding domain and directs mitochondrial localisation of RAB5, which subsequently leads to recruitment of RAB7 by the MON1/CCZ1 complex[1]. As already mentioned in the discussion (p. 12), ubiquitination of the Rab27A GTPase activating protein alpha (TBC1D10A) is reduced in the brain of Parkin KO mouse compared to controls[35], suggesting a possible connection of Rab27A with regulatory mechanisms that are linked with mitochondrial damage and dysfunction. While this an interesting avenue to explore, in this paper we will not follow up further on the mechanism of mitochondrial recruitment of Rab27A.

Author response table 1.

Rab27A interactome. Proteins co-immunoprecipitated with mScarlet-Rab27A vs mScarlet expressing control. The data show average of three replicates.

Gene ID	logFC	P.Value	Protein ID
SYTL1	6.51279398	2.58011E-07	Q8IYJ3
SYTL4	9.462240971	5.37442E-07	Q96C24
RAB27A	9.964034476	0.000225708	P51159
PHKA1	1.901649808	0.00024689	P46020
SYTL5	3.382670586	0.00028503	Q8TDW5
RPN1	1.842817754	0.000618174	P04843
SYTL2	2.787103426	0.000976248	Q9HCH5
SYTL3	1.763916791	0.001231698	Q4VX76
YWHAB	1.324625725	0.001792747	P31946
KPNA4	-2.119041679	0.001819937	O00629
KPNA2	-1.316606494	0.002674273	P52292
XPO7	1.881758901	0.00434815	Q9UIA9
H3F3C	-1.014289683	0.005676851	Q6NXT2
FTSJ3	-1.536695759	0.013027871	Q8IY81
HSPA5	-0.696530058	0.013830063	P11021
GCN1L1	1.282942068	0.014007173	Q92616
SEC23A	-1.154781691	0.014551903	Q15436
YWHAE	1.051069572	0.014721005	P62258
CSE1L	1.573274711	0.015215159	P55060
PRKDC	1.203932332	0.015522477	P78527
HSD17B4	0.622782422	0.018684219	P51659
TUBA1C	0.757418802	0.021056742	Q9BQE3
ATP5A1	1.652450437	0.021124762	P25705
ACADVL	1.487591887	0.023527244	P49748
SYNE1	1.484495661	0.023619887	Q8NF91
TUBA1B	0.869686638	0.026093033	P68363
KHNYN	0.530428593	0.032980211	O15037
STIP1	-1.003028534	0.037684326	P31948
RNF213	2.063787445	0.041437396	Q63HN8
MACF1	-0.558906019	0.041690413	Q9UPN3
BANF1	-2.961226325	0.047019044	O75531
AGL	-1.021197131	0.047045989	P35573

To investigate the role of SYTL5 in the context of ACC, we acquired the NCI-H295R cell line isolated from the adrenal gland of an adrenal cancer patient. The cells were cultured as recommended from ATCC using DMEM/F-12 supplemented with NuSerum and ITS +premix. It is important to note that the H295R cells were adapted to grow as an adherent monolayer from the H295 cell line which grows in suspension. However, there can still be many viable H295R cells in the media.

We attempted to conduct OCR and ECAR measurements using the Seahorse XF upon knockdown of SYTL5 and/or Rab27A in H295R cells. For these assays, it is essential that the cells be seeded in a monolayer at 70-90% confluency with no cell clusters[4]. Poor adhesion of

the cells can cause inaccurate measurements by the analyser. Unfortunately, the results between the five replicates we carried out were highly inconsistent, the same knockdown produced trends in opposite directions in different replicates. This is likely due to problems with seeding the cells. Despite our best efforts to optimise seeding number, and pre-coating the plate with poly-D-lysine[5] we observed poor attachment of cells and inability to form a monolayer.

To study the localisation of SYTL5 and Rab27A in an ACC model, we transduced the H295R cells with lentiviral particles to overexpress pLVX-SV40-mScarlet-I-Rab27A and pLVX-CMV-SYTL5-EGFP-3xFLAG. Again, this proved unsuccessful after numerous attempts at optimising transduction.

These issues limited our investigation into the role of SYTL5 in ACC to the cortisol assay (Supplementary Figure 6). For this the H295R cells were an appropriate model as they are able to produce an array of adrenal cortex steroids[6] including cortisol[7]. In this assay, measurements are taken from cell culture supernatants, so the confluency of the cells does not prevent consistent results as the cortisol concentration was normalised to total protein per sample. With this assay we were able to rule out a role for SYTL5 and Rab27A in the secretion of cortisol.

Another consideration when investigating the involvement of SYTL5 in ACC, is that in general ACC cells should have a low expression of SYTL5 as is seen from the patient expression data (Figure 6B).

The reviewer also writes “Furthermore, images and results supporting the major conclusions need to be improved.”. We have tried several times, without success, to generate U2OS cells with CRISPR/Cas9-mediated C-terminal tagging of endogenous SYTL5 with mNeonGreen, using an approach that has been successfully implemented in the lab for other genes. This is likely due to a lack of suitable sgRNAs targeting the C-terminal region of SYTL5, which have a low predicted efficiency score and a large number of predicted off-target sites in the human genome including several other gene exons and introns (see Author response image 2).

We have also included new data (Supplementary Figure 4B) showing that some of the hypoxia-induced SYTL5-Rab27A-positive vesicles stain positive for the autophagy markers p62 and LC3B when inhibiting lysosomal degradation, further strengthening our data that SYTL5 and Rab27A function as positive regulators of mitophagy.

> ***Reviewer #2 (Public review):***
>
> *Summary:*
>
> *The authors provide convincing evidence that Rab27 and STYL5 work together to regulate mitochondrial activity and homeostasis.*
>
> *Strengths:*
>
> *The development of models that allow the function to be dissected, and the rigorous approach and testing of mitochondrial activity.*
>
> *Weaknesses:*
>
> *There may be unknown redundancies in both pathways in which Rab27 and SYTL5 are working which could confound the interpretation of the results.*
>
> *Suggestions for revision:*
>
> *Given that Rab27A and SYTL5 are members of protein families it would be important to exclude any possible functional redundancies coming from Rab27B expression or one of*

> *the other SYTL family members. For Rab27 this would be straightforward to test in the assays shown in Figure 4 and Supplementary Figure 5. For SYTL5 it might be sufficient to include some discussion about this possibility.*

We thank the reviewer for pointing out the potential redundancy issue for Rab27A and SYTL5. There are multiple studies demonstrating the redundancy between Rab27A and Rab27B. For example, in a study of the disease Griscelli syndrome, caused by Rab27A loss of function, expression of either Rab27A or Rab27B rescues the healthy phenotype indicating redundancy[8]. This redundancy however applies to certain function and cell types. In fact, in a study regarding hair growth, knockdown of Rab27B had the opposite effect to knockdown of Rab27A[9].

In this paper, we conducted all assays in U2OS cells, in which the expression of Rab27B is very low. Human Protein Atlas reports expression of 0.5nTPM for Rab27B, compared to 18.4nTPM for Rab27A. We also observed this low level of expression of Rab27B compared to Rab27A by qPCR in U2OS cells. Therefore, there would be very little endogenous Rab27B expression in cells depleted of Rab27A (with siRNA or KO). In line with this, Rab27B peptides were not detected in our SYTL5 interactome MS data (Table 1 in paper). Moreover, as Rab27A depletion inhibits mitochondrial recruitment of SYTL5 and mitophagy, it is not likely that Rab27B provides a functional redundancy. It is possible that Rab27B overexpression could rescue mitochondrial localisation of SYTL5 in Rab27A KO cells, but this was not tested as we do not have any evidence for a role of Rab27B in these cells. Taken together, we believe our data imply that Rab27B is very unlikely to provide any functional redundancy to Rab27A in our experiments.

For the SYTL family, all five members are Rab27 effectors, binding to Rab27 through their SHD domain. Together with Rab27, all SYTL's have been implicated in exocytosis in different cell types. For example, SYTL1 in exocytosis of azurophilic granules from neutrophils[10], SYTL2 in secretion of glucagon granules from pancreatic α cells[11], SYTL3 in secretion of lytic granules from cytotoxic T lymphocytes[12], SYTL4 in exocytosis of dense hormone containing granules from endocrine cells[13] and SYTL5 in secretion of the RANKL cytokine from osteoblasts[14]. This indicates a potential for redundancy through their binding to Rab27 and function in vesicle secretion/trafficking. However, one study found that different Rab27 effectors have distinct functions at different stages of exocytosis[15].

Very little known about redundancy or hierarchy between these proteins. Differences in function may be due to the variation in gene expression profile across tissues for the different SYTL's (see Author response image 1 below). SYTL5 is enriched in the brain unlike the others, suggesting possible tissue specific functions. There are also differences in the binding affinities and calcium sensitivities of the C2iA and C2B domains between the SYTL proteins[16].

Author response image 1.

GTEx Multi Gene Query for SYTL1-5

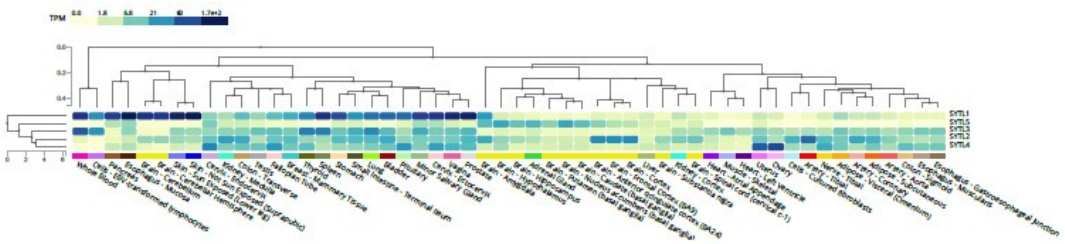

All five SYTL's are expressed in the U2OS cell line with nTPMs according to Human Protein Atlas of SYTL1: 7.5, SYTL2: 13.4, SYTL3:14.2, SYTL4: 8.7, SYTL5: 4.8. In line with this, in the Rab27A interactome, when comparing cells overexpressing mScarlet-Rab27A with control cells, we detected all five SYTL's as specific Rab27A-interacting proteins (see Author response table 1 above). Whereas, in the SYTL5 interactome we did not detect any other SYTL protein (table 1 in paper), confirming that they do not form a complex with SYTL5.

We have included the following text in the discussion (p. 12): "SYTL5 and Rab27A are both members of protein families, suggesting possible functional redundancies from Rab27B or one of the other SYTL isoforms. While Rab27B has a very low expression in U2OS cells, all five SYTL's are expressed. However, when knocking out or knocking down SYTL5 and Rab27A we observe significant effects that we presume would be negated if their isoforms were providing functional redundancies. Moreover, we did not detect any other SYTL protein or Rab27B in the SYTL5 interactome, confirming that they do not form a complex with SYTL5."

> *Suggestions for Discussion:*
>
> *Both Rab27A and STYL5 localize to other membranes, including the endolysosomal compartments. How do the authors envisage the mechanism or cellular modifications that allow these proteins, either individually or in complex to function also to regulate mitochondrial funcYon? It would be interesYng to have some views.*

We agree that it would be interesting to better understand the mechanism involved in modulation of the localisation and function of SYTL5 and Rab27A at different cellular compartments, including the mitochondria. Here, we have shown that SYTL5 recruitment to the mitochondria involves coincidence detection, as both its lipid-binding C2 domains and the Rab27A-binding SHD domain are required (Figure 1G-H). Both these domains also seem required for localisation of SYTL5 to vesicles, and we can only speculate that binding to different lipids (Figure 1F) may regulate SYTL5 localisation. Additionally, we find that mitochondrial recruitment of SYTL5 is dependent on the GTPase activity and mitochondrial localisation of Rab27A (Figure 2D-E). However, this seems also the case for vesicular recruitment of SYTL5, although a few SYTL5-Rab27A (T23N) positive vesicles were seen (Figure 2E).

To characterise the mechanisms involved in mitochondrial localisation of Rab27A, we have performed mass spectrometry analysis to identify the interactome of Rab27A (see Author response table 1 above). U2OS cells with stable expression of mScarlet-Rab27A or mScarlet only were subjected to immunoprecipitation, followed by MS analysis. Of the 32 significant Rab27A-interacting hits (compared to control), two of the hits localise in the inner mitochondrial membrane (IMM); ATP synthase F(1) complex subunit alpha (P25705), and mitochondrial very long-chain specific acyl-CoA dehydrogenase (VLCAD)(P49748). However, as these IMM proteins are not likely involved in mitochondrial recruitment of Rab27A, observed under basal conditions, we chose not to include these data in the manuscript.

It is known that other RAB proteins are recruited to the mitochondria by regulation of their GTPase activity. During parkin-mediated mitophagy, RABGEF1 (a guanine nucleotide exchange factor) is recruited through its ubiquitin-binding domain and directs mitochondrial localisation of RAB5, which subsequently leads to recruitment of RAB7 by the MON1/CCZ1 GEF complex[1]. As already mentioned in the discussion (p.12), ubiquitination of the Rab27A GTPase activating protein alpha (TBC1D10A) is reduced in the brain of Parkin KO mouse compared to controls[35], suggesting a possible connection of Rab27A with regulatory mechanisms that are linked with mitochondrial damage and dysfunction. While this an interesting avenue to explore, it is beyond the scope of this paper.

Our data suggest that SYTL5 functions as a negative regulator of the Warburg effect, the switch from OXPHOS to glycolysis. While both SYTL5 and Rab27A seem required for mitophagy of selective mitochondrial components, and their depletion leading to reduced mitochondrial respiration and ATP production, only depletion of SYTL5 caused a switch to glycolysis. The mechanisms involved are unclear, but we found several proteins linked to the cellular response to oxidative stress, reactive oxygen species metabolic process, regulation of mitochondrion organisation and protein insertion into mitochondrial membrane to be enriched in the SYTL5 interactome (Figure 3A and C).

We have addressed this comment in the discussion on p.12

> ***Reviewer #3 (Public review):***
>
> *Summary:*
>
> *In the manuscript by Lapao et al., the authors uncover a role for the Rab27A effector protein SYTL5 in regulating mitochondrial function and turnover. The authors find that SYTL5 localizes to mitochondria in a Rab27A-dependent way and that loss of SYTL5 (or Rab27A) impairs lysosomal turnover of an inner mitochondrial membrane mitophagy reporter but not a matrix-based one. As the authors see no co-localization of GFP/mScarlet tagged versions of SYTL5 or Rab27A with LC3 or p62, they propose that lysosomal turnover is independent of the conventional autophagy machinery. Finally, the authors go on to show that loss of SYTL5 impacts mitochondrial respiration and ECAR and as such may influence the Warburg effect and tumorigenesis. Of relevance here, the authors go on to show that SYTL5 expression is reduced in adrenocortical carcinomas and this correlates with reduced survival rates.*
>
> *Strengths:*
>
> *There are clearly interesting and new findings here that will be relevant to those following mitochondrial function, the endocytic pathway, and cancer metabolism.*
>
> *Weaknesses:*
>
> *The data feel somewhat preliminary in that the conclusions rely on exogenously expressed proteins and reporters, which do not always align.*
>
> *As the authors note there are no commercially available antibodies that recognize endogenous SYTL5, hence they have had to stably express GFP-tagged versions. However, it appears that the level of expression dictates co-localization from the examples the authors give (though it is hard to tell as there is a lack of any kind of quantitation for all the fluorescent figures). Therefore, the authors may wish to generate an antibody themselves or tag the endogenous protein using CRISPR.*

We agree that the level of SYTL5 expression is likely to affect its localisation. As suggested by the reviewer, we have tried hard, without success, to generated U2OS cells with CRISPR knock-in of a mNeonGreen tag at the C-terminus of endogenous SYTL5, using an approach that has been successfully implemented in the lab for other genes. This is likely due to a lack of suitable sgRNAs targeting the C-terminal region of SYTL5, which have a low predicted efficiency score and a large number of predicted off-target sites in the human genome including several other gene exons and introns (see Author response image 2).

Author response image 2.

Overview of sgRNAs targeting the C-terminal region of SYTL5

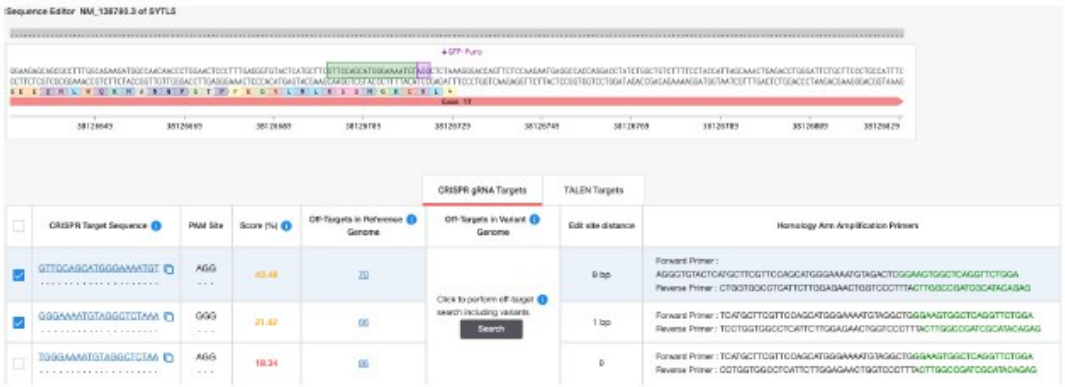

Although the SYTL5 expression level might affect its cellular localization, we also found the mitochondrial localisation of SYTL5-EGFP to be strongly increased in cells co-expressing mScarletRab27A, supporting our findings of Rab27A-mediated mitochondrial recruitment of SYTL5. We have also included new data (Supplementary Figure 4B) showing that some of the hypoxia-induced SYTL5Rab27A-positive vesicles stain positive for the autophagy markers p62 and LC3B when inhibiting lysosomal degradation, further strengthening our data that SYTL5 and Rab27A function as positive regulators of mitophagy.

> *In relation to quantitation, the authors found that SYTL5 localizes to multiple compartments or potentially a few compartments that are positive for multiple markers. Some quantitation here would be very useful as it might inform on function.*

We find that SYTL5-EGFP localizes to mitochondria, lysosomes and the plasma membrane in U2OS cells with stable expression of SYTL5-EGFP and in SYTL5/Rab27A double knock-out cells rescued with SYTL5EGFP and mScralet-Rab27A. We also see colocalization of SYTL5-EGFP with endogenous p62, LC3 and LAMP1 upon induction of mitophagy. However, as these cell lines comprise a heterogenous pool with high variability we do not believe that quantification of the overexpressing cell lines would provide beneficial information in this scenario. As described above, we have tried several times to generate SYTL5 knock-in cells without success.

> *The authors find that upon hypoxia/hypoxia-like conditions that punctate structures of SYTL5 and Rab27A form that are positive for Mitotracker, and that a very specific mitophagy assay based on pSu9-Halo system is impaired by siRNA of SYTL5/Rab27A, but another, distinct mitophagy assay (Matrix EGFP-mCherry) shows no change. I think this work would strongly benefit from some measurements with endogenous mitochondrial proteins, both via immunofluorescence and western blot-based flux assays.*

In addition to the western blotting for different endogenous ETC proteins showing significantly increased levels of MTCO1 in cells depleted of SYTL5 and/or Rab27A (Figure 5E-F), we have now blotted for the endogenous mitochondrial proteins, COXIV and BNIP3L, in DFP and DMOG conditions upon knockdown of SYTL5 and/or Rab27A (Figure 5G and Supplementary Figure 5A). Although there was a trend towards increased levels, we did not see any significant changes in total COXIV or BNIP3L levels when SYTL5, Rab27A or both are knocked down compared to siControl. Blotting for endogenous mitochondrial proteins is however not the optimum readout for mitophagy. A change in mitochondrial protein level does not necessarily result from mitophagy, as other factors such as mitochondrial biogenesis and changes in translation can also have an effect. Mitophagy is a dynamic process, which is why we utilise assays such as the HaloTag and mCherry-EGFP double tag as these indicate flux in the pathway. Additionally, as mitochondrial proteins have different half-lives, with

many long-lived mitochondrial proteins[17], differences in turnover rates of endogenous proteins make the results more difficult to interpret.

> *A really interesting aspect is the apparent independence of this mitophagy pathway on the conventional autophagy machinery. However, this is only based on a lack of co-localization between p62or LC3 with LAMP1 and GFP/mScarlet tagged SYTL5/Rab27A. However, I would not expect them to greatly colocalize in lysosomes as both the p62 and LC3 will become rapidly degraded, while the eGFP and mScarlet tags are relatively resistant to lysosomal hydrolysis. -/+ a lysosome inhibitor might help here and ideally, the functional mitophagy assays should be repeated in autophagy KOs.*

We thank the reviewer for this suggestion. We have now repeated the colocalisation studies in cells treated with DFP with the addition of bafilomycin A1 (BafA1) to inhibit the lysosomal V-ATPase. Indeed, we find that a few of the SYTL5/Rab27A/MitoTracker positive structures also stain positive for p62 and LC3 (Supplementary Figure 4B). As expected, the occurrence of these structures was rare, as BafA1 was only added for the last 4 hrs of the 24 hr DFP treatment. However, we cannot exclude the possibility that there are two different populations of these vesicles.

> *The link to tumorigenesis and cancer survival is very interesYng but it is not clear if this is due to the mitochondrially-related aspects of SYTL5 and Rab27A. For example, increased ECAR is seen in the SYTL5 KO cells but not in the Rab27A KO cells (Fig.5D), implying that mitochondrial localization of SYTL5 is not required for the ECAR effect. More work to strengthen the link between the two sections in the paper would help with future direcYons and impact with respect to future cancer treatment avenues to explore.*

We agree that the role of SYTL5 in ACC requires future investigation. While we observe reduced OXPHOS levels in both SYTL5 and Rab27A KO cells (Figure 5B), glycolysis was only increased in SYTL5 KO cells (Figure 5D). We believe this indicates that Rab27A is being negatively regulated by SYTL5, as ECAR was unchanged in both the Rab27A KO and Rab27A/SYTL5 dKO cells. This suggests that Rab27A is required for the increase in ECAR when SYTL5 is depleted, therefore SYTL5 negatively regulates Rab27A. The mechanism involved is unclear, but we found several proteins linked to the cellular response to oxidative stress, reactive oxygen species metabolic process, regulation of mitochondrion organisation and protein insertion into mitochondrial membrane to be enriched in the SYTL5 interactome (Figure 3A and C).

To investigate the link to cancer further, we tested the effect of knockdown of SYTL5 and/or Rab27A on the levels of mitochondrial ROS. ROS levels were measured by flow cytometry using the MitoSOX Red dye, together with the MitoTracker Green dye to normalise ROS levels to the total mitochondria. Cells were treated with the antioxidant N-acetylcysteine (NAC)[18] as a negative control and menadione as a positive control, as menadione induces ROS production via redox cycling[19]. We must consider that there is also a lot of autofluorescence from cells that makes it impossible to get a level of ‘zero ROS’ in this experiment. We did not see a change in ROS with knockdown of SYTL5 and/or Rab27A compared to the NAC treated or siControl samples (see Author response image 3 below). The menadione samples confirm the success of the experiment as ROS accumulated in these cells. Thus, based on this, we do not believe that low SYTL5 expression would affect ROS levels in ACC tumours.

Author response image 3.

Mitochondrial ROS production normalised to total mitochondria

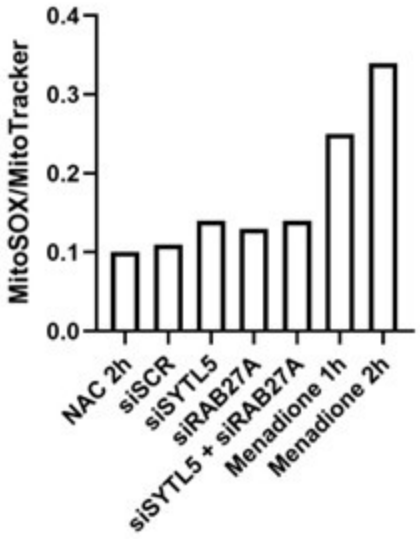

As discussed in our response to Reviewer #1, we tried hard to characterise the role of SYTL5 in the context of ACC using the NCI-H295R cell line isolated from the adrenal gland of an adrenal cancer patient. We attempted to conduct OCR and ECAR measurements using the Seahorse XF upon knockdown of SYTL5 and/or Rab27A in H295R cells without success, due to poor attachment of the cells and inability to form a monolayer. We also transduced the H295R cells with lentiviral particles to overexpress pLVX-SV40-mScarlet-I-Rab27A and pLVX-CMV-SYTL5-EGFP-3xFLAG to study the localisation of SYTL5 and Rab27A in an ACC model. Again, this proved unsuccessful after numerous attempts at optimising the transduction. These issues limited our investigation into the role of SYTL5 in ACC to the cortisol assay (Supplementary Figure 6). For this the H295R cells were an appropriate model as they are able to produce an array of adrenal cortex steroids[6] including cortisol[7] In this assay, measurements are taken from cell culture supernatants, so the confluency of the cells does not prevent consistent results as the cortisol concentration was normalised to total protein per sample. With this assay we were able to rule out a role for SYTL5 and Rab27A in the secretion of cortisol.

Another consideration when investigating the involvement of SYTL5 in ACC, is that in general ACC cells should have a low expression of SYTL5 as is seen from the patient expression data (Figure 6B).

Further studies into the link between SYTL5/Rab27A and cancer are beyond the scope of this paper as we are limited to the tools and expertise available in the lab.

References

(1) Yamano, K. et al. Endosomal Rab cycles regulate Parkin-mediated mitophagy. eLife 7 (2018). https://doi.org:10.7554/eLife.31326

(2) Carré, M. et al. Tubulin is an inherent component of mitochondrial membranes that interacts with the voltage-dependent anion channel. The Journal of biological chemistry 277, 33664-33669 (2002). https://doi.org:10.1074/jbc.M203834200

(3) Hoogerheide, D. P. et al. Structural features and lipid binding domain of tubulin on biomimetic mitochondrial membranes. Proceedings of the National Academy of Sciences 114, E3622-E3631 (2017). https://doi.org:10.1073/pnas.1619806114

(4) Plitzko, B. & Loesgen, S. Measurement of Oxygen Consumption Rate (OCR) and Extracellular Acidification Rate (ECAR) in Culture Cells for Assessment of the Energy Metabolism. Bio Protoc 8, e2850 (2018). https://doi.org:10.21769/BioProtoc2850

(5) Yavin, E. & Yavin, Z. Attachment and culture of dissociated cells from rat embryo cerebral hemispheres on polylysine-coated surface. The Journal of cell biology 62, 540-546 (1974). https://doi.org:10.1083/jcb.62.2.540

(6) Wang, T. & Rainey, W. E. Human adrenocortical carcinoma cell lines. Mol Cell Endocrinol 351, 5865 (2012). https://doi.org:10.1016/j.mce.2011.08.041

(7) Rainey, W. E. et al. Regulation of human adrenal carcinoma cell (NCI-H295) production of C19 steroids. J Clin Endocrinol Metab 77, 731-737 (1993). https://doi.org:10.1210/jcem.77.3.8396576

(8) Barral, D. C. et al. Functional redundancy of Rab27 proteins and the pathogenesis of Griscelli syndrome. J. Clin. Invest. 110, 247-257 (2002). https://doi.org:10.1172/jci15058

(9) Ku, K. E., Choi, N. & Sung, J. H. Inhibition of Rab27a and Rab27b Has Opposite Effects on the Regulation of Hair Cycle and Hair Growth. Int. J. Mol. Sci. 21 (2020). https://doi.org:10.3390/ijms21165672

(10) Johnson, J. L., Monfregola, J., Napolitano, G., Kiosses, W. B. & Catz, S. D. Vesicular trafficking through cortical actin during exocytosis is regulated by the Rab27a effector JFC1/Slp1 and the RhoA-GTPase–activating protein Gem-interacting protein. Mol. Biol. Cell 23, 1902-1916 (2012). https://doi.org:10.1091/mbc.e11-12-1001

(11) Yu, M. et al. Exophilin4/Slp2-a targets glucagon granules to the plasma membrane through unique Ca2+-inhibitory phospholipid-binding activity of the C2A domain. Mol. Biol. Cell 18, 688696 (2007). https://doi.org:10.1091/mbc.e06-10-0914

(12) Kurowska, M. et al. Terminal transport of lyXc granules to the immune synapse is mediated by the kinesin-1/Slp3/Rab27a complex. Blood 119, 3879-3889 (2012). https://doi.org:10.1182/blood-2011-09-382556

(13) Zhao, S., Torii, S., Yokota-Hashimoto, H., Takeuchi, T. & Izumi, T. Involvement of Rab27b in the regulated secretion of pituitary hormones. Endocrinology 143, 1817-1824 (2002). https://doi.org:10.1210/endo.143.5.8823

(14) Kariya, Y. et al. Rab27a and Rab27b are involved in stimulation-dependent RANKL release from secretory lysosomes in osteoblastic cells. J Bone Miner Res 26, 689-703 (2011). https://doi.org:10.1002/jbmr.268

(15) Zhao, K. et al. Functional hierarchy among different Rab27 effectors involved in secretory granule exocytosis. Elife 12 (2023). https://doi.org:10.7554/eLife.82821

(16) Izumi, T. Physiological roles of Rab27 effectors in regulated exocytosis. Endocr J 54, 649-657 (2007). https://doi.org:10.1507/endocrj.kr-78

(17) Bomba-Warczak, E. & Savas, J. N. Long-lived mitochondrial proteins and why they exist. Trends in cell biology 32, 646-654 (2022). https://doi.org:10.1016/j.tcb.2022.02.001

(18) Curtin, J. F., Donovan, M. & Cotter, T. G. Regulation and measurement of oxidative stress in apoptosis. Journal of Immunological Methods 265, 49-72 (2002). https://doi.org:https://doi.org/10.1016/S0022-1759(02)00070-4

(19) Criddle, D. N. et al. Menadione-induced Reative Oxygen Species Generation via Redox Cycling Promotes Apoptosis of Murine Pancreatic Acinar Cells. Journal of Biological

Chemistry 281, 40485-40492 (2006). https://doi.org:https://doi.org/10.1074/jbc.M607704200

https://doi.org/10.7554/eLife.105541.2.sa0